ANTIBACTERIAL PROPERTIES OF ZINC OXIDE NANOPARTICLES ON *Klebsiella pneumoniae* ATCC 13883

By

TAN SIN TY

A project report submitted to the Department of
Allied Health Sciences
Faculty of Science
Universiti Tunku Abdul Rahman
In partial fulfilment of the requirements for the degree of
Bachelor of Science (Hons) Biomedical Science

May 2022

ABSTRACT

ANTIBACTERIAL PROPERTIES OF ZINC OXIDE NANOPARTICLES ON *Klebsiella pneumoniae* ATCC 13883

Tan Sin Ty

The overuse of antibiotics to treat *Klebsiella pneumoniae* infection has led to the development of multidrug-resistant strains, stimulating the study of the nanomaterial as an effective antibacterial alternative to conventional antibiotics. The objectives of our study were to evaluate the antibacterial activity of ten zinc oxide nanoparticle (ZnO NP) concentrations against Gram-negative bacterium *K. pneumoniae* by determining growth inhibitory effects via microbroth dilution method, bacterial surface functional groups involved in attaching ZnO NPs to bacteria by Fourier transform infrared (FTIR) spectroscopy, and the morphological alterations caused by ZnO NPs through the scanning electron microscope with energy-dispersive X-ray spectroscopy (SEM-EDX). All the tested ZnO NP concentrations showed statistically significant inhibition against *K. pneumoniae* in turbidity and INT assays. The average percentage of growth inhibition reported on *K. pneumoniae* was 5, 13, 17, 23, 29, 36, 46, 65, 83, and 87% for 5, 10, 20, 40, 80, 160, 320, 640, 1280, and 2560 µg/ mL of ZnO NPs, respectively. Besides, the MIC value was determined to be 2560 µg/mL using an iodonitrotetrazolium chloride (INT)

assay. The FTIR spectrum exhibited the involvement of bacterial surface polysaccharides, proteins, glycogen, and phospholipids in the interaction of ZnO NPs with bacterial cells. Furthermore, SEM analysis showed ZnO NP aggregation on bacterial cells, roughening of the cell surface, membrane damage and rupture, cell shrinkage and distortion. The EDX analysis verified the adsorption of ZnO NPs on *K. pneumoniae* surface. The attachment of ZnO NPs to *K. pneumoniae* and the subsequent morphological damages are the possible causes behind the inhibitory effects of ZnO NPs on *K. pneumoniae* growth. Overall, our current study confirmed the dose-dependent antibacterial activity of ZnO NPs against *K. pneumoniae* via the interaction of NPs with *K. pneumoniae* envelope, which caused alterations in cell membrane integrity that might have resulted in cell death.

ACKNOWLEDGEMENT

First and foremost, I would like to express my deepest gratitude to my project supervisor, **Dr. Sinouvassane Djearamane**, for his guidance, encouragement, and patience.

I would also like to extend my heartiest appreciation to **Universiti Tunku Abdul Rahman (UTAR)** for giving me this golden opportunity to do research. This project will not have been possible without the sufficient facilities and equipment available in the laboratories.

My special regards pay to **laboratory officers**, namely Mr. Saravanan a/l Sivasangaran, Ms. Hemaroopini a/p Subramaniam, Ms. Fatin Masturah Binti Mohd Isa, Ms. Natrah Binti Khalid, Mr. Ooh Keng Fei, and Mr. Seou Chi Kien, for offering me with technical assistance.

I gratefully acknowledge the help of **my seniors and supportive friends** who share knowledge selflessly with me to achieve my project goals.

Last but not least, my sincere thanks also go to **my family**, who understood and supported me morally throughout the project.

DECLARATION

I hereby declare that this final year project report is based on my original work except for the quotations and citations which have been acknowledged. I also declare that it has not been previously or concurrently submitted for any other degree at UTAR or other institutions.

(TAN SIN TY)

APPROVAL SHEET

This final year project report entitled "**ANTIBACTERIAL PROPERTIESOF ZINC OXIDE NANOPARTICLES ON *Klebsiella pneumoniae* ATCC 13883"** was prepared by TAN SIN TY and submitted as partial fulfilment of the requirements for the degree of Bachelor of Science (Hons) BiomedicalScience at Universiti Tunku Abdul Rahman.

Approved by:

_____

Date: 21/04/2022

(Dr. Sinouvassane Djearamane)

Supervisor

Department of Allied Health Sciences

Faculty of Science

Universiti Tunku Abdul Rahman

FACULTY OF SCIENCE

UNIVERSITI TUNKU ABDUL RAHMAN

Date: 21/04/2022

PERMISSION SHEET

It is hereby certified that **TAN SIN TY** (ID No: **19ADB04386**) has completed this final year project report entitled "ANTIBACTERIAL PROPERTY OF ZINC OXIDE NANOPARTICLES ON *Klebsiella pneumoniae* ATCC 13883" under the supervision of Dr. Sinouvassane Djearamane from the Department of Allied Health Science, Faculty of Science.

I hereby give permission to the University to upload the softcopy of my final year project report in pdf format into the UTAR Institutional Repository, which may be made accessible to the UTAR community and public.

Yours truly,

(TAN SIN TY)

TABLE OF CONTENTS

LISTS OF TABLES

LIST OF FIGURES

LIST OF ABBREVIATIONS

ANOVA	One-way Analysis of Variance
ATCC	American type culture collection
CA	Community acquired
CHL	Chloramphenicol
cKp	Classical *K. pneumoniae*
CPS	Polysaccharide capsule
EDX	Energy Dispersive X-ray
ERY	Erythromycin
ESBL	Extended-spectrum β-lactamase
FTIR	Fourier Transform Infrared
GRAS	Generally Recognised as Safe
h	Hour
HA	Hospital acquired
H_2O_2	Hydrogen Peroxide
hvKp	Hypervirulent *K. pneumoniae*
INT	2-(4-iodophenyl)-3-(4-nitrophenyl)-5-phenyl-2H-tetrazolium Chloride
KAN	Kanamycin Sulfate
KBr	Potassium Bromide
KPC	*K. pneumoniae* Carbapenemase
LPS	Lipopolysaccharide
MBC	Minimum Bactericidal Concentration
MDR	Multidrug Resistance
MIC	Minimum Inhibitory Concentration
min	Minute

MNPs	Metal Nanoparticles
NPs	Nanoparticles
OD	Optical Density
OMPs	Outer Membrane Proteins
PLA	Pyogenic Liver Abscess
PBS	Phosphate Buffered Saline
ROS	Reactive Oxygen Species
SEM	Scanning Electron Microscope
STM	Scanning Tunneling Microscope
SPSS	Statistical Package for the Social Sciences
TCH	Tetracycline Hydrochloride
UTIs	Urinary Tract Infections
Zn^{2+}	Zinc Ions
ZnO	Zinc Oxide

CHAPTER 1

INTRODUCTION

1.1 Research Background

Klebsiella pneumoniae commonly causes hospital- (HA) and community-acquired (CA) infections like wound infections, pneumonia, septicaemia, urinary tract infections (UTIs), and pyogenic liver abscess (PLA) (Ko et al., 2002; Magill et al., 2014; Spagnolo et al., 2014; Paczosa and Mecsas, 2016). The increasing incidence of *K. pneumoniae* carbapenemase (KPC)-producing and extended-spectrum β-lactamase (ESBL) strains of *K. pneumoniae* in the healthcare system are a worldwide challenge (Diaz, et al., 2009). Recently, *K. pneumoniae* has gained much attention due to its disease severity, multidrug resistance (MDR), and treatment difficulty (Ranjbar et al., 2019, 2016ab). Therefore, the development of alternative treatments against infection by multidrug-resistant *K. pneumoniae* has become increasingly important.

Nanotechnology is an encouraging field that involves applying materials smaller than 100 nanometers in the agricultural, food, healthcare, cosmetics, medical and diagnostic industries (Silvera Batista et al., 2015). In 1959, Richard Zsigmondy coined the term "nanometer" to characterise particle size. The term "nanotechnology" was first used by Norio Taniguchi to describe semiconductor processes at a nanometer scale. Nanotechnology was opened up in 1981 with the invention of the scanning tunneling microscope (STM), which

visualizes individual atoms, by Gerd Binnig and Heinrich Rohrer (National Nanotechnology Initiative [NHI], 2011).

Physiochemical and biological properties of inorganic nanomaterials over their bulk phase make them effective antimicrobials (Fiedot et al., 2017; Nie et al., 2020). Zinc oxide nanoparticle (ZnO NP) stands out from other metallic nanomaterials as antibacterial agents as it offers broader protection against major foodborne pathogens, gram-positive and gram-negative bacteria, cheaper, safer, white, and UV-blocking (Mohd Yusof et al., 2021). ZnO is classified as a “Generally Recognised as Safe” (GRAS) compound by the Food and Drug Administration (FDA, 2022). The large surface-to-volume ratio of ZnO NPs renders their applications as antimicrobial agents in food packaging (Ahmadi et al., 2020), topical creams such as antifungal ointments (Sogne et al., 2017), and animal feed (Ye et al., 2020).

The antibacterial activity of small ZnO NP concentration ranges was studied by scientists worldwide (Buzea et al., 2007; Jones et al., 2008; Webster and Seil, 2012). However, the surface interaction, and agglomeration of ZnO NPs on the bacterial cell envelopes were less studied. There was limited information regarding the antibacterial potential of ZnO NPson *K. pneumoniae.*

In this study, the economical and time-saving broth microdilution assay was used to assess the antibacterial activity of ten ZnO NP concentrations against *K. pneumoniae*. Besides, the contact and associated damage done by ZnO NPs on bacterial cells were demonstrated.

1.2 Research Objectives

The aim of this study is to evaluate the antibacterial activity of ZnO NPs against *K. pneumoniae* by examining the growth inhibition, surface interaction and accumulation of ZnO NPs on *K. pneumoniae* envelope.

Specific research objectives are:

1) To determine the bacteriostatic and bactericidal effect of ZnO NPs on *K. pneumoniae* ATCC 13883.

2) To study the interaction of ZnO NPs with *K. pneumoniae* ATCC 13883 surface biomolecules.

3) To observe the cellular accumulation and morphological alteration in *K. pneumoniae* ATCC 13883 after treatment with ZnO NPs.

CHAPTER 2

LITERATURE REVIEW

2.1 Overview of *Klebsiella pneumoniae*

2.1.1 General Properties

Carl Friedlander first described *K. pneumoniae* in 1882 as an organism found in the lungs of deceased pneumonia patients (Friedlaender, 1882). This bacillus was initially known as Friedlander's bacterium (Merino et al., 1992). *Klebsiella pneumoniae*, a Gram-negative rod that belongs to the *Enterobacteriaceae* family, is non-motile, facultatively anaerobic, and encapsulated (Janda and Abbott, 2006). These bacteria are present in the environment, including soil and water. Also, they colonise the medical devices, mucosal surfaces of the mammalian gastrointestinal (GI) and oropharyngeal mucosa (Rock et al., 2014). The organism undergoes lactose fermentation for metabolic purposes, resulting in highly mucoid colonies on carbohydrate-rich media due to the production of a luxuriant polysaccharide capsule (Donnenberg, 2015).

2.1.2 Virulence Factors

As presented in **Figure 2.1**, the siderophore-producing ability, fimbriae or pili, lipopolysaccharide (LPS), and polysaccharide capsule (CPS) mainly confer K. pneumoniae pathogenicity (Favre-Bonte et al., 1999; Shon et al., 2013). It was recently found that outer membrane proteins (OMPs), efflux pumps, iron

acquisition systems, and gene clusters related to allantoin degradation are also crucial factors that contribute to the pathogen's virulence (Paczosa and Mecsas, 2016).

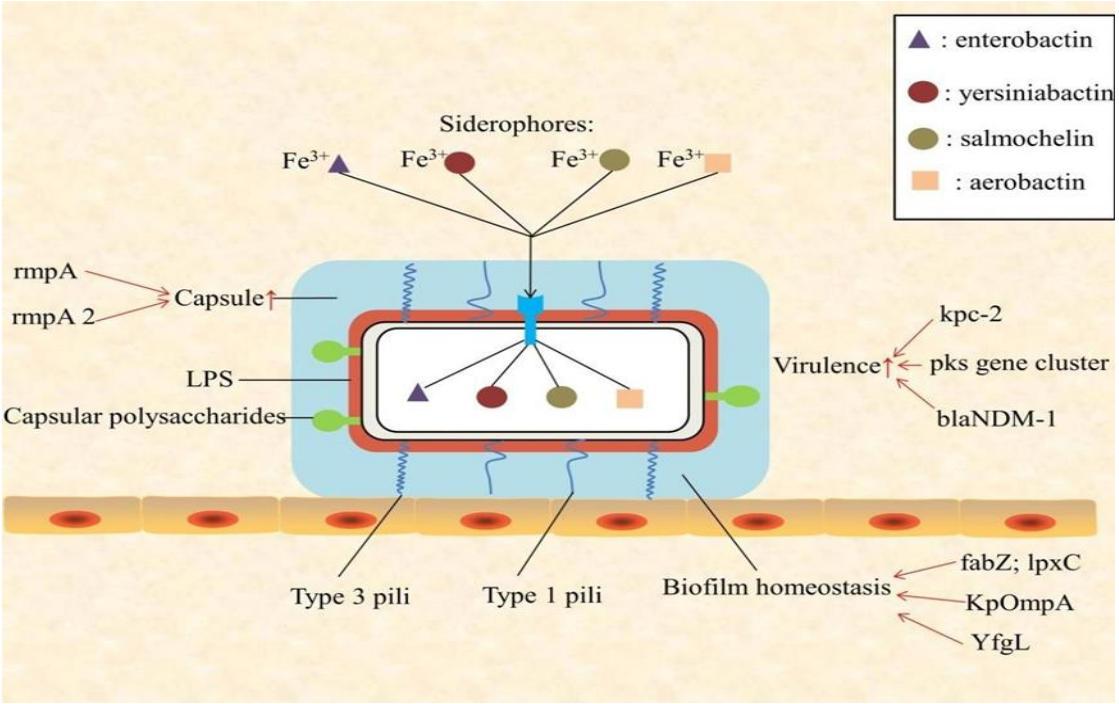

Figure 2.1: Pictorial representation of virulence factors and biofilm homeostasis in *K. pneumoniae* (adopted from Wang et al., 2020).

The iron supply is necessary for tissue-invasive *K. pneumoniae* growth and pathogenesis (Fang *et al*., 2007). *Klebsiella pneumoniae* secretes one or more of the following siderophores: enterobactin, salmochelin, yersiniabactin, and aerobactin, to chelate iron with high affinity and overcome iron scarcity in mammalian hosts (Li et al., 2014). Aerobactin has the lowest affinity for iron, while enterobactin has the highest (Brock et al., 1991; Perry et al., 1999). The host molecule lipocalin-2 is unable to inhibit all siderophores except for enterobactin (Paczosa and Mecsas, 2016).

Both classical (*cKp*) and hypervirulent (*hvKp*) strains contain enterobactin, which is a primary iron carrier with the highest affinity for iron (Tarkkanen et al., 1992; Koczura and Kaznowski, 2003). Enterobactin is dominantly involved in an iron acquisition under more iron-depleting conditions (Lawlor et al., 2007). Salmochelin is more prevalent in *hvKp* strains and is associated with severe community-acquired infections, such as pyogenic liver abscesses (Fischbach et al., 2005, 2006).

The structures of yersiniabactin and aerobactin are different from those of enterobactin and salmochelin. Transferrin reduces the functionality of yersiniabactin. Yersiniabactin enables *K. pneumoniae* to maintain respiratory infection and generate pneumonia (Bachman *et al*., 2011). The aerobactin enhances the virulence of less virulent *K. pneumoniae* strains (Nassif and Sansonetti, 1986) and is responsible for more than 90% of *hvKp*'s siderophore activity (Russo et al., 2014, 2015).

Compared to non-virulent strains, *hvKp* strains produce larger, more activated iron-absorbing molecules, which may contribute to their virulence and pathogenicity (Russo et al., 2011).

Both *cKp* and *hvKp* express fimbrial adhesins, namely, type 1 and type 3 fimbriae, which play a vital role in infection and biofilm formation (Stahlhut et al., 2012). Filamentous type 1 fimbriae mediate uroepithelial cell adhesion, as

well as biofilm formation in the bladder wall, plants, and medical devices (Klemm and Schembri, 2000). Helix-like type 3 fimbriae are essential for *K. pneumoniae* biofilm production and adhesion to several human cell types, plants, and abiotic surfaces (Khater et al., 2015).

The LPS, a component of the Gram-negative bacterial outer membrane made up of the lipid A, core oligosaccharide, and O antigen is produced by both strains of *K. pneumoniae.* Lipid A, or endotoxin, is a potent activator of inflammation. An altered lipid A becomes less inflammatory and helps *K. pneumoniae* evade innate immunity during infection (Montminy et al., 2006; Llobet et al., 2015). Lipid A modification may affect antibiotic resistance in Klebsiella strains (Llobet *et al*., 2015). In addition, lipid A protects against the bactericidal effects of positively charged antimicrobial peptides (Clements et al., 2007; Llobet et al., 2015).

An O antigen is the outermost domain of LPS that protects against complement. It inhibits the complement activation pathway by blocking C1q's binding to bacteria (Albertí et al., 1993). Additionally, it prevents pore formation by binding C3b away from the target site on the outer bacterial membrane (Merino et al., 1992; Merle et al., 2015). The number of serotypes is about 9 for O antigens (O1 to 9), with O1 being the most common (Hansen et al., 1999).

Klebsiella pneumoniae possesses CPS for adherence to host tissues, biofilm formation, and immune evasion (Li et al., 2014; Sachdeva et al., 2017). Among the serotypes K1 to K78 expressed by *cKp* strains, K1 and K2 are associated with increased pathogenicity (Trautmann et al., 1997; Edwards and Fife, 1952; Edmunds, 1954; Behera, 2010). The *hvKp* strains make a hypercapsule, which overproduces CPS (Nassif et al., 1989; Russo et al., 2011).

Due to the presence of this capsule at the cell surface, this pathogen appears large on gram stain and is resistant to many host defense mechanisms (Qureshi, 2019). *Klebsiella pneumoniae* is protected from opsonophagocytosis, binding and ingestion by macrophages (Cortes et al., 2002), neutrophils (Pan et al., 2011), dendritic cells (DCs) (Evrard et al., 2010), and epithelial cells (Sahly et al., 2000). Human beta-defensins (HBD-1 to -3) and lactoferrin (LF) are hampered in their bactericidal activity by the binding of CPS distal from the outer membrane (Fang et al., 2004). Besides, CPS prevents complement-mediated lysis and opsonisation by blocking the interaction of complement C3 with the membrane (Simoons-Smit et al., 1986; Tomás et al., 1986; Merino et al., 1992; Albertí et al., 1993; Fang et al., 2004; Clements et al., 2008). As measured by reduced production of reactive oxygen species (ROS), interleukin-8 and IL-6, and tumor necrosis factor-alpha (TNF-α), it prevents the robust immune reaction by activating the nucleotide-binding and oligomerization domain (NOD) pathway and preventing LPS from being recognized by immune cells (Evrard et al., 2000; Yoshida et al., 2001).

2.1.3 Clinical Significance

The dissemination of *K. pneumoniae* from mucosae can cause life-threatening urinary tract (UTIs), respiratory tract, blood, and wound site infections (Podschun and Ullmann, 1998; Magill et al., 2014). It accounts for about one-third of all Gram-negative infections. Neonates, the elderly, and immunocompromised patients in medical facilities are at a higher risk of contracting *K. pneumoniae* (Magill et al., 2014). The *hvKp* strains are typical community-associated and systemic infectious agents in relatively healthy individuals. Conversely, *cKp* strains usually cause serious healthcare-associated infections (Russo et al., 2014).

Approximately 11.8% of hospital-acquired pneumonia (HAP) results from K. pneumoniae infection (Magill et al., 2014). According to Podschun and Ullmann (1998), mortality rates for *K. pneumoniae* pneumonia can reach 50%. *Klebsiella pneumoniae* is the second leading cause of UTIs and bacteraemia by Gram-negative bacteria (Podschun and Ullmann, 1998; Magill et al., 2014). Ninety-seven percent of nosocomial UTIs are catheter-associated UTIs (CAUTIs) (Murphy and Clegg, 2012).

Higher mortality risk factors for *K. pneumoniae* bacteraemia include intensive care unit (ICU) admission, alcoholism, malignancy, pneumonia, urinary catheter or ventilator requirement (Meatherall et al., 2009; Chetcuti Zammit et al., 2014). Treatment with corticosteroids, chemotherapy, and transplantation puts patients at risk for nosocomial infection (Korvick et al., 1991). The

gastrointestinal tract of hospitalized patients and the hands of healthcare workers can serve as reservoirs for the transmission of bacteria, and they are responsible for multiple hospital outbreaks (Gupta 2002).

2.1.4 Common Treatment

Klebsiella infections are commonly treated with antibiotics. To select the most appropriate antimicrobial agent against *K. pneumoniae*, antimicrobial susceptibility testing must be performed in conjunction with microbiological diagnosis.

Carbapenems are preferred for treating extended-spectrum beta-lactamase-(ESBL-)producing *K. pneumoniae* infection, as these antibiotics are highly resistant to hydrolysis by β-lactamases and have retained efficacy against ESBL-producing organisms (Colodner et al., 2004). Treatment options for MDR *K. pneumoniae* include combinations of aminoglycosides, tigecycline, and older antibiotics. Colistin was considered a "last resort" treatment of CRKP infections.

2.1.5 Multidrug Resistance Problem

Klebsiella pneumoniae tops the Global Priority List of Antibiotic-Resistant Bacteria published by the World Health Organization (WHO) in 2017. With its multidrug-resistant (MDR), high morbidity and mortality, and limited

treatment options, *K. pneumoniae* infections are associated with higher treatment costs (Al-Saiym et al., 2015).

Selective pressure resulting from increased carbapenem use has resulted in the development of carbapenem-resistant *K. pneumoniae* (CRKP). These microbes produce *K. pneumoniae* carbapenemase (KPC), causing clinical issue and challenging treatment (Nordmann et al., 2009). It is alarming that the incidence of colistin-resistant and tigecycline-resistant *K. pneumoniae* is rising (Marchaim et al., 2011; van Duin et al., 2015).

The misuse and uncontrolled use of antimicrobials to treat *K. pneumoniae* infections may cause its increased MDR strain (Fuzi, Rodriguez Baño, and Toth, 2020). Ngoi et al. (2021) found that ESBL-producing *K. pneumoniae* causing UTIs in Malaysia were highly resistant to commonly prescribed antibiotics such as third- and fourth-generation cephalosporins. In Malaysia, CRKPs have increased tremendously from 0.3% in 2011 to 2.8% in 2015 due to the rapid dissemination of the New Delhi Metallo-β-lactamase -1 (NMD-1) gene (Lee et al., 2017). O'Neill and his team (2014) estimated that, by 2050, antimicrobial-resistant infections would kill 10 million people per year- more than cancer mortality- unless action is taken.

2.2 Zinc oxide nanoparticles

2.2.1 Biomedical application

The properties of ZnO NPs, an inorganic metallic nanoparticle (MNP), such as antibacterial, antifungal, anticancer, antidiabetic, and anti-inflammatory, render their vast application. Besides, ZnO NPs do not interact with most therapeutically active compounds (Sahdev et al., 2013). The ZnO NPs are relatively inexpensive, more biocompatible (Azizi et al., 2014), and less toxic to humans than silver (Ag) and titanium dioxide (TiO_2) (Garcia et al., 2018).

Their anti-diabetic effects attribute to their ability to reduce oxidative stress in diabetes (Pandey and Rizvi, 2009; Choudhary et al., 2011; Saravanan et al., 2011; Ademiluyi and Oboh, 2013). Furthermore, ZnO NPs show higher photocatalytic activity and are naturally antibacterial (Mishra et al., 2017; Fernando et al., 2018). Studies claimed that the high photocatalytic characteristics of ZnO NPs increase their efficiency as antibacterial and antifungal agents (Cioffi and Rai, 2012; Dizaj et al., 2014). The ZnO NP application in wound recovery is promising because of their strong antimicrobial and anti-inflammatory properties, while zinc helps in re-epithelialization process (Lansdown et al., 2007). Rasha et al. (2021) demonstrated that an KPC-infection wound treatment with ZnO NPs could reduce inflammation compared with the antibiotic imipenem. The U.S. FDA has classified ZnO NPs as safe in treating bacterial infection-associated tissue damage (Rao, T. et al., 2019).

The ROS-inducing ability of ZnO NPs render their antibacterial and anticancer activities (Condello et al., 2016). Interestingly, ZnO NPs were proved to exert selective toxicity against cancer cells through ROS production, mitochondrial membrane potential destruction, and thus apoptosis (Sasidharan et al., 2011; Wahab et al., 2013). Electrostatic interactions between anionic cancer cells and cationic ZnO NPs facilitate their uptake, phagocytosis, and cytotoxicity (Rasmussen et al., 2010). While other MNPs like iron oxide nanoparticles also demonstrate anticancer activities, there is a lack of evidence indicating that they are antimicrobial or UV absorbent (Mishra et al., 2017).

2.2.2 Antibacterial Properties

Due to the resurgence of infectious diseases and the prevalence of antibiotic-resistant strains, particularly among Gram-negative bacteria, nanotechnology has become increasingly relevant in the biomedical and pharmaceutical industries as an alternative antibacterial agent (Desselberger, 2000).

Researchers (Ghasemi and Jalal; Sarwar et al., 2016) discovered that ZnO NPs increase the antibacterial activity of antibiotics, suggesting a synergistic effect between ZnO NPs and antibiotics as an effective alternative for treating bacterial infections. The simultaneous action of antimicrobial mechanisms renders resistance development to nanoparticles extremely unlikely (Pelgrift & Friedman, 2013).

Generally, Gram-positive bacteria were more vulnerable to ZnO than Gram-negative (Umar et al., 2018; Banerjee et al., 2021). As shown in **Figure 2.2**, the peptidoglycan layer of Gram-positive cells is thicker than Gram-negative bacteria. However, high lipid and protein contents in Gram-negative bacterial outer membranes make them more resistant to nanoparticles and metal ions. The cell wall of Gram- positive bacteria is composed of almost 60% teichoic acids (Sobhanifar et al., 2015), serving as an anion site that attracts the Zn2+, causing them to be more vulnerable to ZnO NPs (Esmailzadeh et al., 2016; Dimapilis et al., 2018). **Table 2.1** shows the antibacterial properties of ZnO NPs against various bacteria.

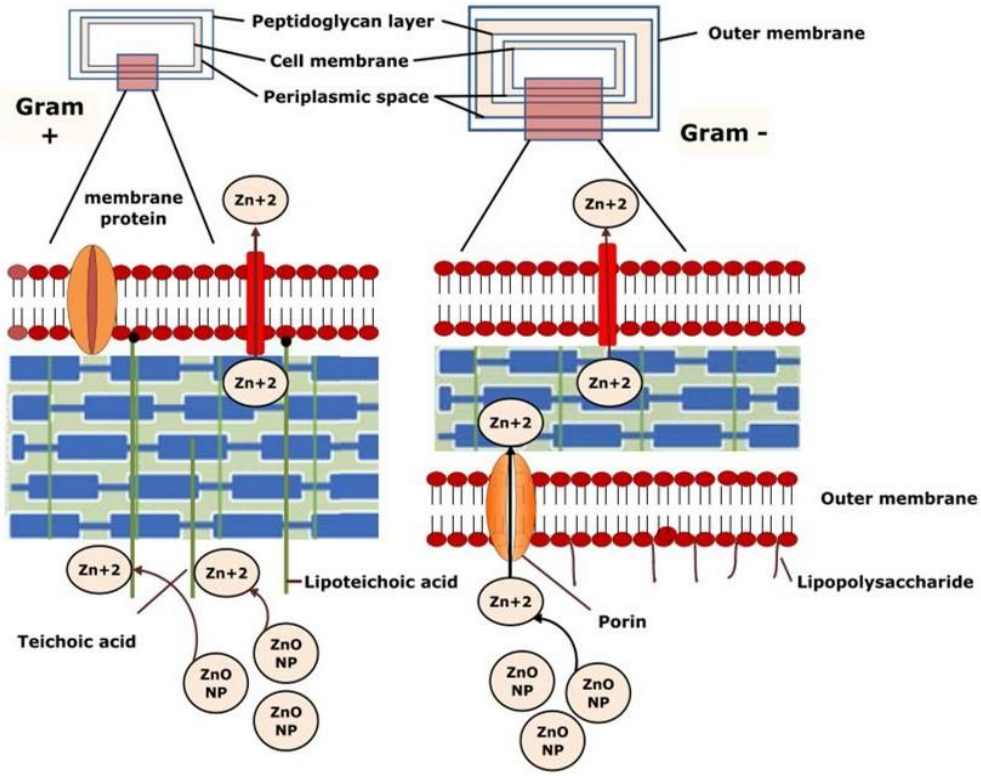

Figure 2.2 Interaction of ZnO NPs with Gram-positive and Gram-negative bacteria (Adopted from Happy Agarwal et al., 2018).

Table 2.1 Antibacterial properties of ZnO NPs.

Organism	Concentration of ZnO NPs (µg/mL)	Methods	Results	References
(+): *Bacillus cereus* and *Staphylococcus aureus* (-): *Pseudomonas aeruginosa* and *Salmonella Typhimurium*	50, 500, 1000, and 2000	Broth dilution • MBC and MIC	for both *S. aureus* and *S. Typhimurium*, MIC: 50 µg/mL, MBC: 500 µg/mL	(Souza et al., 2019)
(+): *Staphylococcus aureus* (-): *Escherichia coli* and *Salmonella* spp.	• MIC and MBC: 10 to 5000 • Agar Well Diffusion Method: 1000 , 2000, 3000, 4000, and 5000	• MIC and MBC • Agar Well Diffusion Method	5000 µg/mL showed highest inhibition zone, *S. aureus* was more susceptible MIC: • *Salmonella spp.*: 80 µg/mL • *E. coli*: 60 µg/mL • *S. aureus*: 30 µg/mL MBC: • *Salmonella spp.*: 160 µg/mL • *E. coli*: 140 µg/mL • *S. aureus*: 100 µg/mL	(Mohd Yusof et al., 2021)

Foot note: (+): Gram-positive bacteria; (-): Gram-negative bacteria

Table 2.1 Antibacterial properties of ZnO NPs (continued).

Organism	Concentration of ZnO NPs (µg/mL)	Methods	Results	References
(+): *Enterococcus faecalis* (-): *Escherichia coli*	7, 15, 31, 62, 125, 250, 500 and 1000	MIC_{50}	S3 (small particle sizes) showed better antibacterial activities against both bacteria compared to S4 as shown by its lower MIC_{50} values.	(Mohamad Sukri et al., 2019)
(+): *Bacillus subtilis* and *Staphylococcus epidermidis*	10000	agar well diffusion technique	-strong antibacterial activity of ZnO NPs against *B. subtilis*, *S. epidermidis*, and *E. cloacae* with ZOI values of 17, 14 and 16 mm, respectively	(Hassanein et al., 2021)
(-): *Enterobacter cloacae* and *Escherichia coli*			-moderate activity against *E. coli* (ZOI = 10 mm).	
(+): *Streptococcus pyogenes*	20, 40, 60, 80, 100	Turbidity measurement	Growth of bacteria cells with NPs was lower than the growth of bacteria without NPs. Growth of bacteria decreased 6, 22.6, 43.4, 48.4 and 48% as the concentration of NPs increased.	(Bhuyan et al., 2015)

Foot note: (+): Gram-positive bacteria; (-): Gram-negative bacteria

Table 2.1 Antibacterial properties of ZnO NPs (continued).

Organism	**Concentration of ZnO NPs (µg/mL)**	3. **Methods**	**Results**	**References**
(+): *Bacillus subtilis, Staphylococcus aureus* (-): *Pseudomonas aeruginosa, Escherichia coli*	25, 50, 75, 100	MIC	• *P. aeruginosa, B. subtilis* and *E.coli :* 75 µg/mL • *S. aureus:* 100 µg/mL	(Malathi et al., 2021)
(+): *Staphyllococcus aureus*, and *Streptococcus pyogenes* (-): *Pseudomonas aeruginosa*, and *Proteus mirabilis*	25, 50 and 100	disc diffusion technique	• the zone of inhibition was relatively higher for gram negative bacteria (absence of a thick peptidoglycan layer in the cell wall) compared to gram positive bacteria. • 100 µg/mL: the highest zone of inhibition	(Rambabu et al., 2021)

Foot note: (+): Gram-positive bacteria; (-): Gram-negative bacteria

Table 2.1 Antibacterial properties of ZnO NPs (continued).

Organism	Concentration of ZnO NPs (µg/mL)	Methods	Results	References
(+): *Staphylococcus aureus* (-): *Escherichia coli*	50	disc-diffusion method	ZnO NPs has significant antibacterial activities against Gram-negative bacteria than the Gram-positive strain with high selectivity	(Das and Rebecca, 2017)
(+): *Staphylococcus aureus and Bacillus cereus.* (-): *Escherichia coli, Klebsiella pneumoniae, Pseudomonas aeruginosa, Serratia marcescens, Salmonella typhi, Acinetobacter baumannii, Citrobacter freundii, Proteus mirabilis*	160000, 80000, 40000, 20000, 10000, 5000, 2500, 1250, 620, 310, 150, 75	MIC & MBC	MIC • *S. aureus*, *S. marcescens* and *E. coli*: >2500 µg/mL other bacteria: 5000 µg/mL. MBC • *P. aeruginosa*, *A. baumannii*, *K. pneumoniae* and *S. aureus*: 10000 µg/mL • other bacteria: 20000 µg/mL	(Nazoori and Kariminik, 2018)

Foot note: (+): Gram-positive bacteria; (-): Gram-negative bacteria

2.2.3 Toxicity Concern

Through dermal exposure, ZnO NPs do not demonstrate any systemic toxicity, while inhalation exposure is associated with a low level of pulmonary toxicity. Conversely, oral, intravenous, or intraperitoneal exposure to ZnO NPs causes severe toxicity to all major body organs (Singh et al., 2020). Despite their toxic properties, nanoparticles possess inarguable benefits to kill microorganisms for a short contact time (Sanchez-Sanhueza et al., 2018), considering the increasing resistance of microorganisms to conventional antimicrobial agents. The nanoparticles should be coated with biocompatible polymers to minimize the release of toxic Zn^{2+} ions from them by dissolution (Singh et al., 2020). Functionalization of NP surfaces by targeting proteins or chemical groups will make them more selective against the target tissue and reduce side effects on other organs (Qu and Morais, 1999; Singh et al., 2020).

CHAPTER 3

MATERIALS AND METHODS

3.1 Chemicals / Reagents Preparation

3.1.1 Tryptic Soy Agar (TSA)

The TSA was used to culture and maintain *K. pneumoniae* in this study. For TSA preparation, 36 g of TSA powder was weighed using an analytical balance. A volume of 900 mL of distilled water was used to dissolve the powder. The solution was sent to be autoclaved at 121°C for 15 min. The agar solution was then poured into Petri dishes and allowed to solidify in a laminar flow cabinet. Next, the TSA plates were properly sealed with parafilm and stored upside down at room temperature before use.

3.1.2 Tryptic Soy Broth (TSB)

The TSB was used for culturing and broth microdilution assay in this study. To prepare TSB, 27 g of TSB powder was weighed with an analytical balance and dissolved using 900 mL of distilled water. Prior to use, the solution was autoclaved at 121°C for 15 min and then stored at room temperature.

3.1.3 Mueller-Hinton Agar (MHA)

The MHA was used for the antibiotic susceptibility test in this study. For MHA preparation, 15.2 g of MHA powder was weighed using an analytical balance and dissolved using 400 mL of distilled water. The solution was subsequently autoclaved at 121°C for 15 min. The agar solution was then poured into Petri dishes and allowed to solidify inside a laminar flow cabinet. Next, MHA plates were properly sealed with parafilm and stored upside down at room temperature prior to usage.

3.1.4 Zinc Oxide Nanoparticles (ZnO NPs)

The ZnO NP stock solution (5120 μg/mL) was prepared by adding 25.6 mg of ZnO NP powder to 5 mL of TSB, ultra-sonicated for 30 min at 35°C, 37 kHz to get homogenous solution and then was diluted with TSB to prepare the working concentrations of 5, 10, 20 40, 80, 160, 320, 640, 1280, and 2560 μg/mL of ZnO NPs.

3.1.5 Chloramphenicol (CHL), 1.0 mg /mL

Chloramphenicol powder with 0. 03 g was dissolve using 30 mL of ethanol to reach a final concentration of 1.0 mg/mL. The solution was filtered using a 0.45 μm syringe filter into a sterile Scott bottle and stored at -20°C prior to usage.

3.1.6 Erythromycin (ERY), 1.0 mg /mL

Erythromycin powder with 0. 03 g was dissolved using 30 mL of ethanol to reach a final concentration of 1.0 mg/mL. The solution was filtered using a 0.45 µm syringe filter into a sterile Scott bottle and stored at -20°C prior to usage.

3.1.7 Kanamycin sulfate (KAN), 1.0 mg /mL

Kanamycin sulfate powder with 0. 03 g was dissolved in 30 mL of ethanol to obtain a final concentration of 1.0 mg/mL. The solution was filtered using a 0.45 µm syringe filter into a sterile Scott bottle and stored at -20°C prior to usage.

3.1.8 Tetracycline hydrochloride (TCH), 1.0 mg /mL

Tetracycline hydrochloride powder with 0. 03 g was dissolved in 30 mL of ethanol to obtain a final concentration of 1.0 mg/mL. The solution was filtered using a 0.45 µm syringe filter into a sterile Scott bottle and stored at -20°C prior to usage.

3.1.9 Phosphate Buffered Saline (PBS), 1X

A PBS tablet was dissolved by 100 mL of distilled water and autoclaved at 121°C for 15 min.

3.1.10 2-(4-iodophenyl)-3-(4-nitrophenyl)-5-phenyl-2H-tetrazolium chloride (INT) dye, 0.4 mg/ mL

The INT powder, 0.04 g, was dissolved using 10 mL of sterile distilled water and sonicated at 35°C for 30 min, 37 kHz, to mix the solution homogeneously. The solution was filtered using a 0.45 μm syringe filter into a sterile Scott bottle, covered with aluminium foil, and stored at -20 °C before usage.

3.2 Characterization of ZnO NPs

Scanning electron microscope-energy dispersive X-ray (SEM-EDX) analyses were conducted on ZnO nanoparticles powder from Sigma-Aldrich, Malaysia with a particle size of less than 100 nm. The particle size and shape of ZnO NPs were measured by SEM by applying an acceleration voltage of 4 kV and a working distance of 4.7 nm, while the chemical composition of ZnO NPs was determined by EDX (JSM-6701F, JOEL, Japan).

3.3 Overview of Research Methodology

Klebsiella pneumoniae strain American Type Culture Collection (ATCC 13883) was obtained from MicroBioLogics, Inc., USA and was sub-cultured to mid-log phase at the 2 h, and exposed to different ZnO NP concentrations (5, 10, 20, 40, 80, 160, 320, 640, 1280, and 2560 μg/mL) for 24 h. After that, growth inhibition tests (turbidity method and INT assay), FTIR and SEM-EDX analyses were conducted.

3.4 Experimental Procedure

3.4.1 Gram Staining

The bacterial stock was Gram-stained to ensure that the bacterial sample was not contaminated by Gram-positive or non-rod-shaped microorganisms. After air drying and heat fixing, the cell smear was flooded with the crystal violet staining reagent (1 min), mordant (Gram's iodine, 1 min, decolorizing agent (ethanol, 15 s), and counterstain (safranin, 1 min) sequentially. The slide was washed with tap water for 2 s in between these steps. After flooding the slide with safranin, it was washed with tap water until no coloured effluent. The slide was blot dry with absorbent paper, and the result was observed under oil immersion using a light microscope (Gephardt et al., 1981).

3.4.2 Construction of Bacterial Growth Curve

Klebsiella pneumoniae strain ATCC 13883 was grown in TSB and incubated at 200 rpm at 37°C. After an overnight incubation, 100 mL of fresh TSB was added with 2 mL of primary culture and swirled to mix well. A volume of 1 mL of the bacteria culture was used to measure the absorbance at OD_{600} using a spectrophotometer (Genesys 20, Thermo Scientific) for every one-hour interval from zero to seventh and half hour. The procedure was repeated at twenty-fourth, forty-eighth, and seventy-second hour. Same volume of TSB was set as the blank. The OD_{600} reading were then used to plot the bacterial growth curve to identify the bacterial mid-log phase.

3.4.3 Preparation of Bacterial Culture

The stock of *K. pneumoniae* was prepared by inoculating 50 bacterial colonies from the TSA plate into the TSB and incubating them at 37°C for 24 h. After overnight incubation, bacteria culture with an absorbance of 0.013 ± 0.002 was prepared from the stock, followed by 2 h of incubation to reach the mid-log phase at 37°C. Spectrophotometer was set to blank using TSB at 600 nm wavelength. The mid-log phase turbidity of bacterial suspension was adjusted to fall within the absorbance range of 0.080-0.100, which is equivalent to $1x10^8$ CFU/mL.

3.4.4 Disc Diffusion Susceptibility Test

In this study, a disk diffusion test was adopted to identify the appropriate antibiotic to be used as a positive control. The susceptibility of *K. pneumoniae* against antibiotics tetracycline hydrochloride (TCH), chloramphenicol (CHL), kanamycin sulfate (KAN), and erythromycin (ERY) was assessed. These antibiotics were shown to be effective against *K. pneumoniae* isolated from wound tissues (Afreen et al., 2020). A sterile cotton swab was used to swab the mid-log *K. pneumoniae* suspension having an OD_{600} of 0.080-0.100 onto an MHA plate in a back-and-forth motion closely. Then, 6 mm filter paper disks impregnated with 10 µg of antibiotics were placed and pressed gently onto the plate using forceps. Next, the plates were inverted and incubated for 24 h at 37°C. Following incubation, the zone of inhibition diameter was measured to the nearest millimeter using a ruler (Hudzicki, 2009).

3.4.5 Exposure of Bacteria to ZnO NPs

To prevent any contamination from happening, exposure was performed in the laminar flow cabinet. All sterile 96-well plates were labelled correctly as shown in **Figure 3.1**. First, 100 µL of the antibiotic tetracycline hydrochloride (1 mg/mL) was pipetted into wells 12A-C of 96-well plates which serve as the positive control. Then, 100 µL of TSB was pipetted into each well in rows A-C, except for column 11 and 12, and rows F-G, except for column 1, 11 and 12. After that, 200 µL of ZnO NP stock (5120 µg/mL) was pipetted into 11A-C and 11F-H. Then, it was followed by a serial two-fold dilution using a multi-channel micropipette. After serial dilution, 100 µL of solution was discarded from column 2 of the plates. The column 1 only contains 100 µL of TSB served as the negative control for tracking *K. pneumoniae* normal growth without nanoparticles. Finally, 100 µL of bacterial suspension at mid-log phase was added into each well in rows A-C. The final concentrations of ZnO NPs in different wells were 5, 10, 20, 40, 80, 160, 320, 640, 1280, and 2560 µg/mL, respectively. Different concentrations of ZnO NPs in rows F-H act as nanoparticle control to ensure no contamination by bacteria. Wells in rows F-H should not have colour changes after incubating with INT dye as only viable bacteria can cause a change in colouration of the dye. All plates were covered and sealed properly with parafilm and incubated for 24 h at 37°C.

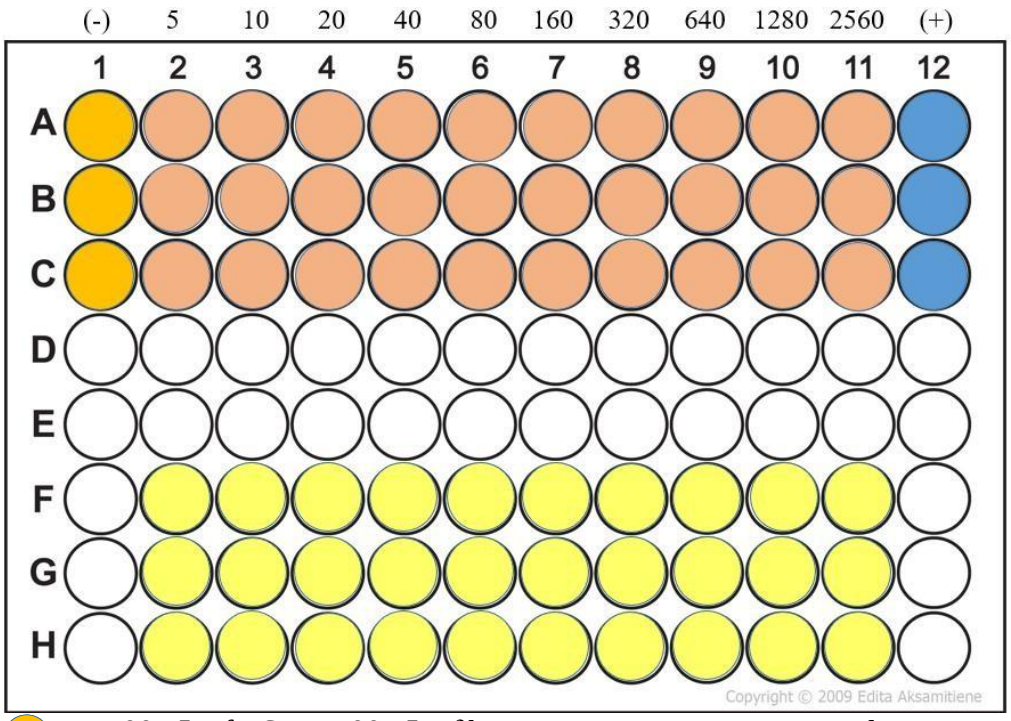

100 µL of TSB + 100 µL of bacteria acts as negative control

100 µL of TSB + 100 µL of bacteria acts as positive control

100 µL of different ZnO NP concentrations + 100 µL of bacteria

100 µL of different ZnO NP concentrations acts as nanoparticle control

Foot note: (-) = negative control; 5, 10, 20, 40, 80, 160, 320, 640, 1280, and 2560 = 5, 10, 20, 40, 80, 160, 320, 640, 1280, and 2560 µg/ mL, respectively; (+) = positive control

Figure 3.1: Design of a 96-well plate for exposing *K. pneumoniae* to ZnO NPs.

3.4.6 Growth Inhibition Tests

3.4.6.1 Turbidity Assay

The turbidity assay enabled the determination of ZnO NP bacteriostatic potential. The turbidity of ZnO NP treated *K. pneumoniae* suspensions were read using the microplate reader (FLUOstar® Omega, Germany) at OD_{600} together with controls incubated at for 24 h at 37°C. The subtraction of ZnO

NP suspension absorbance readings from the test readings, were performed to remove the interference from NPs. The medium for bacteria cell growth, tryptic soy broth (TSB) was used as the blank. Absorbance values were analysed recorded after orbital shaking of 500 rpm for 5 s to observe the percentage of growth inhibition after treating with different ZnO NP concentrations.

The treated bacterial growth inhibition percentage at OD_{600} was calculated using the formula shown below (Liang et al., 2020):

$$I\% = (\mu C - \mu T) / \mu C \times 100$$

Where,

I% = bacterial growth inhibition percentage

μC = mean OD_{600} in negative control

μT = mean OD_{600} in treatment

3.4.6.2 INT Assay as Minimum Inhibitory Concentration (MIC) Assay

The INT assay functioned to determine the MIC of ZnO NPs against *K. pneumoniae*. The MIC is the least antimicrobial concentration that prevents microbial growth. After *K. pneumoniae* was incubated with different ZnO NP concentrations at 37°C for 24 h, 20 μL of 4 mg/ml INT dye was added to the 96-well plate as an indicator of microbial growth. The plate was incubated for

20 min for colour development. Results and observations were recorded after orbital shaking of 500 rpm for 5 s. To remove any interference from NPs, the measured OD_{600} for each concentration of ZnO NPs suspension was subtracted from the test reading. Those wells containing ZnO NP without the addition of bacteria should not have colour change. The wells containing bacteria which remained yellowish colour indicate that the concentration of ZnO NP inhibited bacterial growth, while the wells which showed purple or pink colour indicate the growth of bacteria. The lowest concentration of ZnO NP displaying no visible growth was recorded as the MIC value. This antibacterial assay was carried out in triplicate. The INT assay was done in a dark condition since INT dye is light sensitive. The treated bacterial growth inhibition percentage at OD_{600} was calculated using the same formula shown in **3.4.6.1** (Djeussi et al., 2016).

3.4.6.3 Minimum Bactericidal Concentration (MBC) Assay

MBC is the lowest antimicrobial concentration needed to kill 99.9% of microorganisms. MBC value is the lowest concentration of ZnO NP displaying no colony formation. Based on MIC result, 5 μL of medium was pipetted out from the wells which remained yellowish colour after adding INT along with the negative control into labelled MHA plates and spread evenly with a sterile metal spreader. The parafilm-sealed plates were incubated for 24 h at 37 °C before performing the standard plate count method. After incubation, the number of colonies was counted and recorded.

3.4.7 ZnO NP Interaction with Bacterial Cell Envelope by Fourier Transform Infrared (FTIR) Spectroscopy

The FTIR analysis was done to investigate bacterial cell surface functional groups involved in interaction with ZnO NPs. Twenty-five microliters of negative control and 2560 µg/mL ZnO NP treated *K. pneumoniae* incubated for 24 h were subjected to centrifugation for 10 min at 8000 × *g*. After that, 1X PBS was used to wash the pellets thrice. The pellets were dried using a freeze dryer. The dried sample was mixed with KBr salt powder, hand-pulverized by mortar, and tableted for FTIR measurement (Perkin-Elmer Spectrum RX1, USA).

3.4.8 Scanning Electron Microscope and Energy Dispersive X-ray (SEM-EDX) Analysis

The 2560 µg/mL ZnO NP treated *K. pneumoniae* for 24 h and negative control sample were incubated with 2.5% of glutaraldehyde in PBS for overnight fixing. The next day, the samples were centrifuged and washed three times with 0.01M PBS for 10 min at 8000 × *g*. This washing process was repeated using distilled water. Then, the samples were dehydrated by a series of different concentrations of ethanol (50%, 95% and 99,9%). The dehydration process that used 99.9% of ethanol was repeated three times followed by freeze drying and sputter coating. The samples were analysed under SEM-EDX (JOEL JSM 6710F, Japan).

3.4.9 Statistical Analysis

Statistical analysis was aimed to identify the variances when different concentrations of ZnO NPs interacted with *K. pneumoniae*. The assays were run in triplicates (n=3) and the sample mean and standard deviation were presented. The one-way ANOVA (SPSS version 24) was used to report the significant antibacterial effects ($p<0.05$).

CHAPTER 4

RESULTS

4.1 ZnO NP Characterization

The morphology of ZnO NP powder was studied with SEM, while EDX analysis helped identify the elements present in ZnO NPs. According to **Figure 4.1(A)**, ZnO NPs consisted of a mixture of spherical and rod shapes. Besides, the average particle size was 86.8 nm, ranging from 63.0 to 100.0 nm. The EDX spectrum in **Figure 4.1(B)** depicted that zinc, oxygen, and carbon molecules were present in the NP powder studied.

(A)

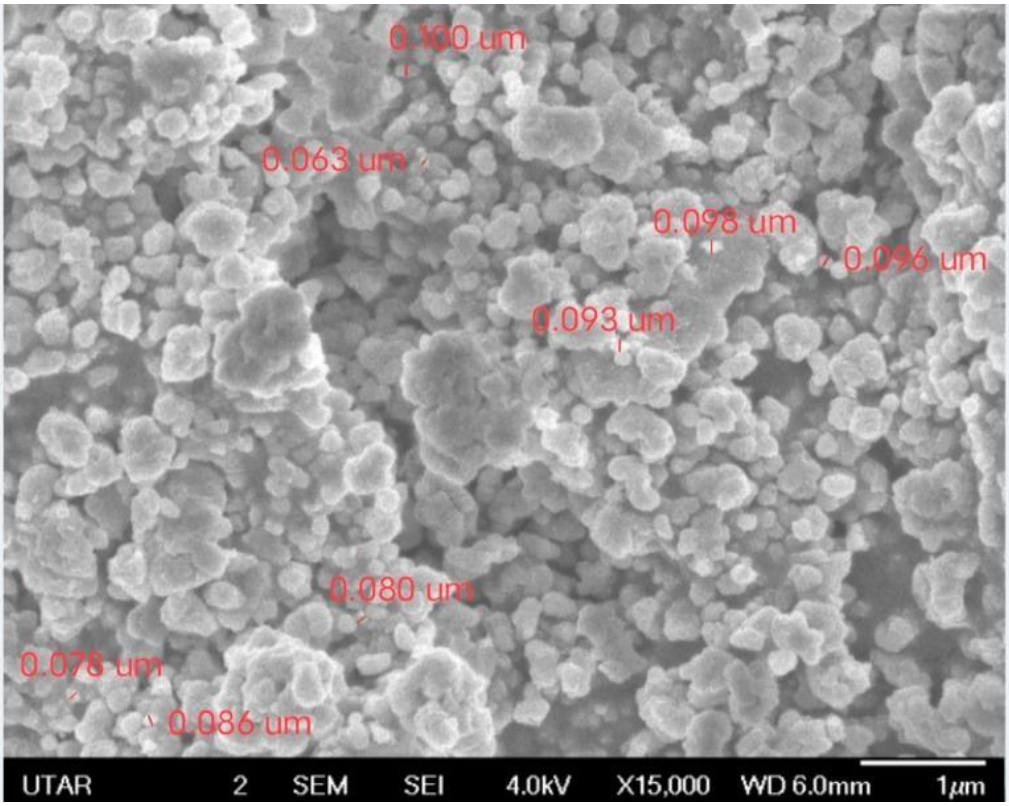

(B)

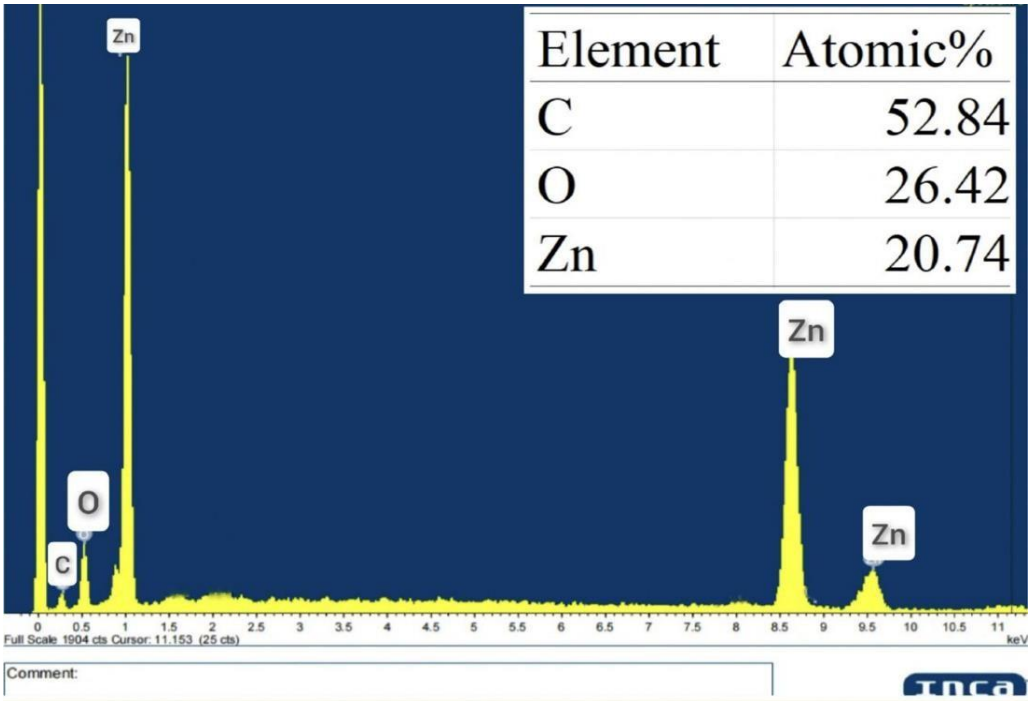

Element	Atomic%
C	52.84
O	26.42
Zn	20.74

Figure 4.1: ZnO NP Characterization under **(A)** SEM with 15,000X magnification. EDX spectrum **(B)** shows that zinc, oxygen, and carbon were present in ZnO NP powder.

4.2 Gram Staining

Gram stain of *K. pneumoniae* showed Gram negative bacilli with no specific arrangement under a light microscope. The positive result confirmed that the bacterial sample was not contaminated by Gram positive or non-rod-shaped microorganisms.

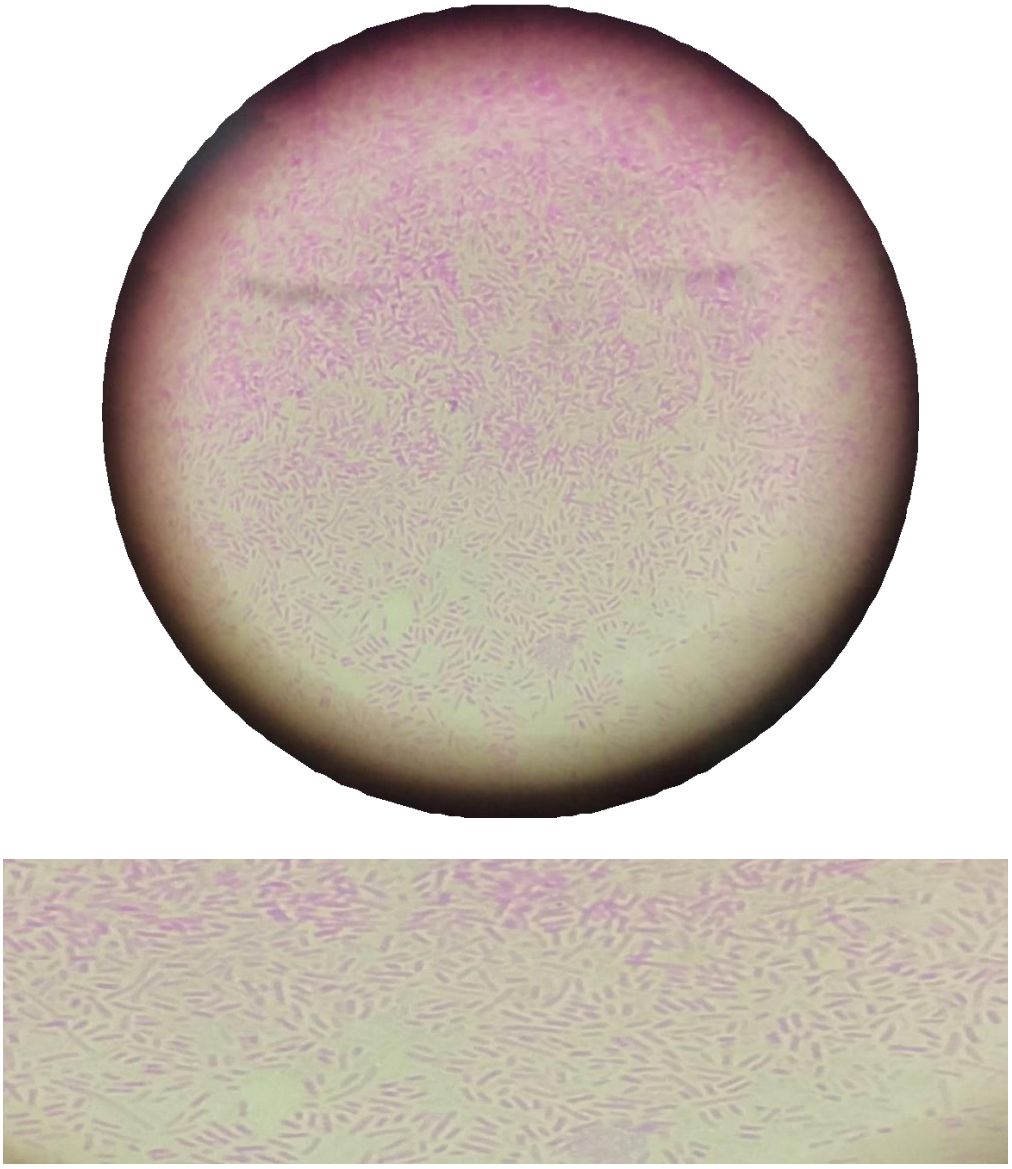

Figure 4.2: Gram-staining micrograph of *K. pneumoniae* with 1,000X oil immersion.

4.3 Bacterial Growth Curve

The growth rate of *Klebsiella pneumoniae* strain ATCC 13883 was assessed by OD_{600} throughout the 72 h of incubation period. The data tabulated in **Table 4.1** demonstrates the growth of *K. pneumoniae,* and these values were used to construct the bacterial growth curves. The bacterial growth curves indicated by OD_{600} increased across the lag phase, exponential phase, stationary phase, and death phase (**Table 4.1** and **Figure 4.3**). The lag phase of the bacteria growth occurred in the first hour of the incubation period. The exponential phase occurred from the first to the third hour, and the mid-log phase was identified as the second hour. The early stationary phase was observed at the 3.5 hours of the incubation period, while the growth of *K. pneumoniae* declined from 24 to 72 h.

Table 4.1: Growth of *K. pneumoniae* strain ATCC 13883 indicated by OD_{600}.

Time (hrs)	**OD_{600}**
0	0.025 ± 0.019
1	0.095 ± 0.007
2	0.416 ± 0.019
3	1.392 ± 0.009
4	1.693 ± 0.023
5	1.855 ± 0.022
6	1.966 ± 0.026
7	2.010 ± 0.063
7.5	2.061 ± 0.108
24	2.353 ± 0.015
48	2.344 ± 0.045
72	2.302 ± 0.152

Mean ± Standard deviation, n=3

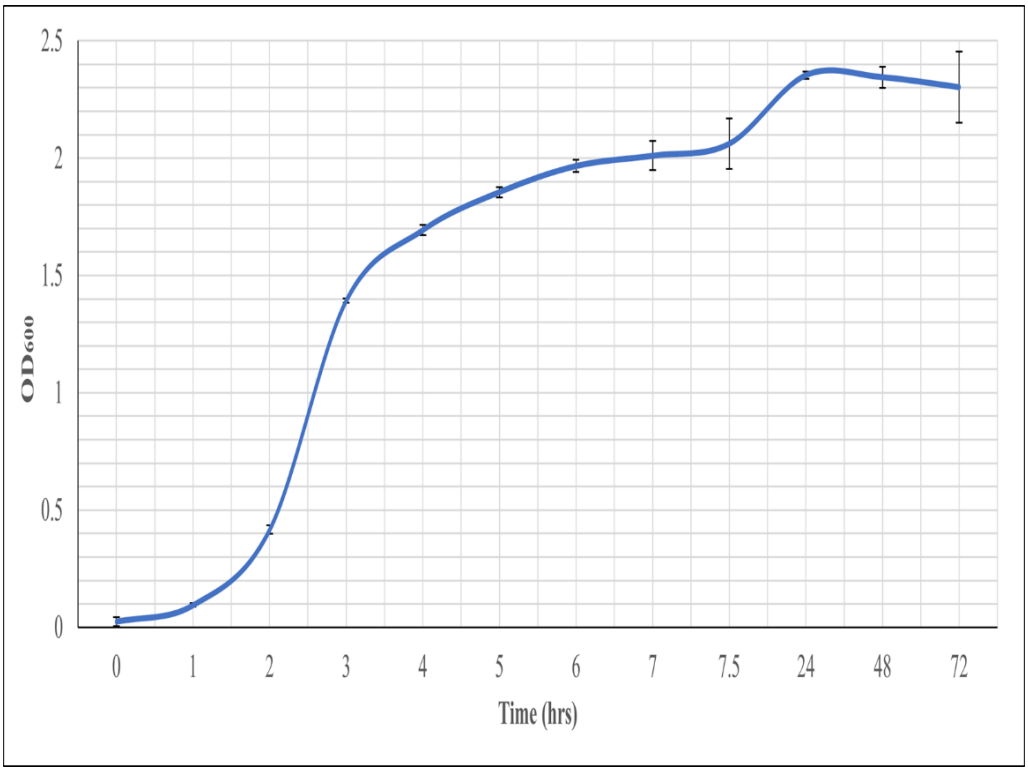

Mean ± Standard deviation, n=3

Figure 4.3: *Klebsiella pneumoniae* growth curve in TSB at 37°C throughout the 72 hours incubation period as measured in OD_{600}. The values plotted are in mean ± standard deviation.

4.4 Disc Diffusion Susceptibility Test

Disc diffusion method was performed to identify and choose the most effective antibiotic against *K. pneumoniae* as the positive control for the following growth inhibition tests. According to **Figure 4.4** and **Table 4.2**, tetracycline hydrochloride produced the largest zone of inhibition (28.23 ± 0.21 mm), followed by chloramphenicol (25.63 ± 0.61 mm), kanamycin sulfate (17.83 ± 0.56 mm), and erythromycin (8.88 ± 0.65 mm). The results observed revealed the highest susceptibility of the bacterium to tetracycline hydrochloride, making the latter a suitable positive control.

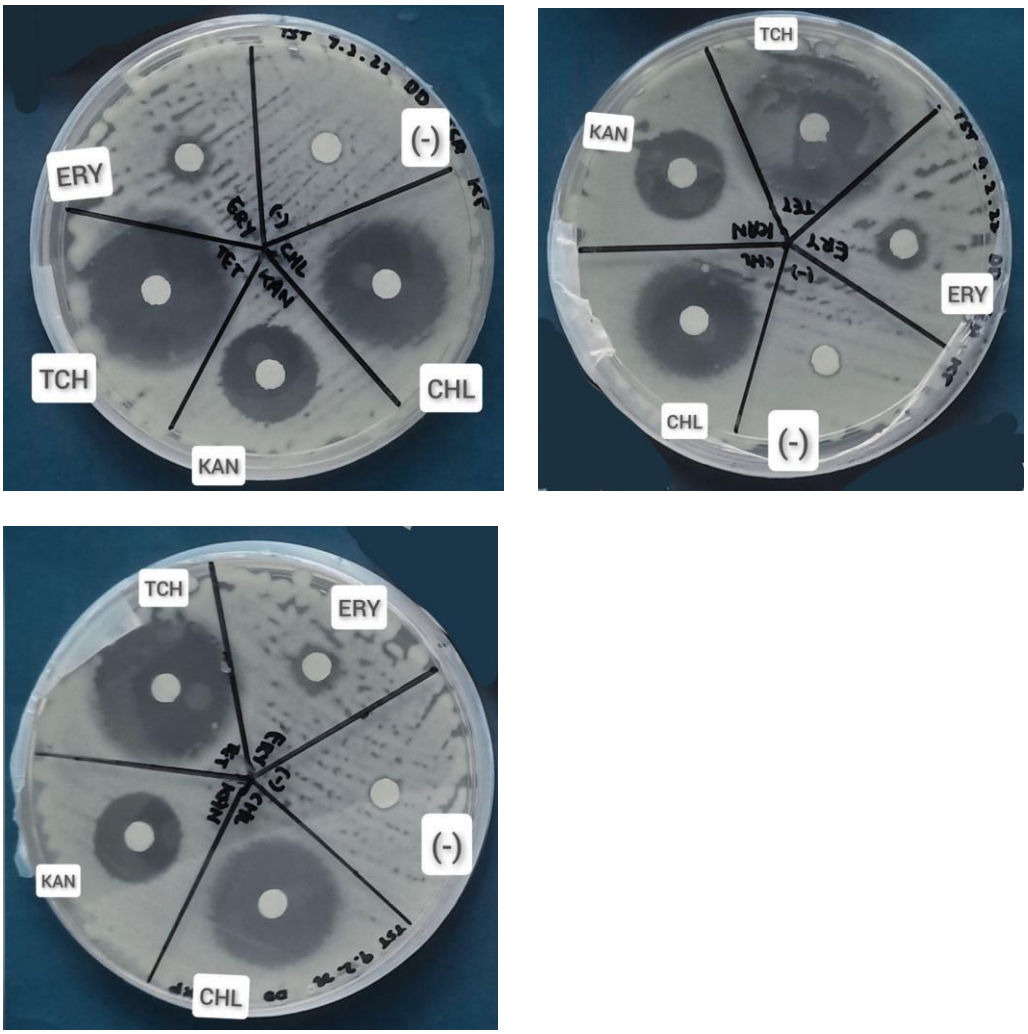

Figure 4.4 Evaluation of the antimicrobial activity of various antibiotics by disc diffusion assay (*CHL* Chloramphenicol, *KAN* Kanamycin sulfate, *TCH* Tetracycline Hydrochloride, *ERY* Erythromycin, *N* Negative control).

Table 4.2 Inhibition zone (ZI) diameters of different antibiotics against *K. pneumoniae*.

Antibiotics	**Zone of inhibition (mm)**
Tetracycline hydrochloride (TCH)	28.23 ± 0.2
Chloramphenicol (CHL)	25.63 ± 0.6
Kanamycin sulfate (KAN)	17.83 ± 0.6
Erythromycin (ERY)	8.88 ± 0.7

Mean ± Standard deviation, n=3

4.5 Growth Inhibition Test

4.5.1 Turbidity Method

The turbidity method was used to measure the optical density of bacteria suspension at OD_{600} at 24 h of incubation with the addition of different ZnO NP concentrations. Antibiotic tetracycline hydrochloride (TCH) with a concentration of 1 mg/mL served as the positive control.

The percentage of growth inhibition of *K. pneumoniae* is presented in **Table 4.3** and **Figure 4.5.** The results showed statistically significant (p <0.05) *K. pneumoniae* growth inhibition by all the tested ZnO NP concentrations at 24 h as compared to the negative control, with the resultant values of 4.67 ± 0.46, 13.27 ± 1.48, 18.78 ± 2.41, 22.40 ± 2.43, 25.60 ± 0.55, 33.86 ± 2.77, 47.84 ± 2.71, 64.11 ± 1.89, 82.20 ± 2.68, 87.39 ± 2.25% for 5, 10, 20, 40, 80, 160, 320, 640, 1280, and 2560 μg/ mL of ZnO NPs, respectively.

Table 4.3: The growth inhibition percentage of *K. pneumoniae* treated by different ZnO NP concentrations and the positive control for 24 h at 37°C in TSB obtained from the turbidity method.

ZnO NP concentration (µg/mL)	**Percentage of growth inhibition (%)**
5	4.89 ± 0.16
10	13.27 ± 1.05
20	18.78 ± 2.41
40	22.40 ± 2.43
80	25.60 ± 0.55
160	33.86 ± 2.77
320	47.84 ± 1.71
640	64.11 ± 1.89
1280	82.20 ± 2.65
2560	87.39 ± 2.25
TCH (1 mg/mL)	93.69 ± 1.24

Mean ± Standard deviation, n=3

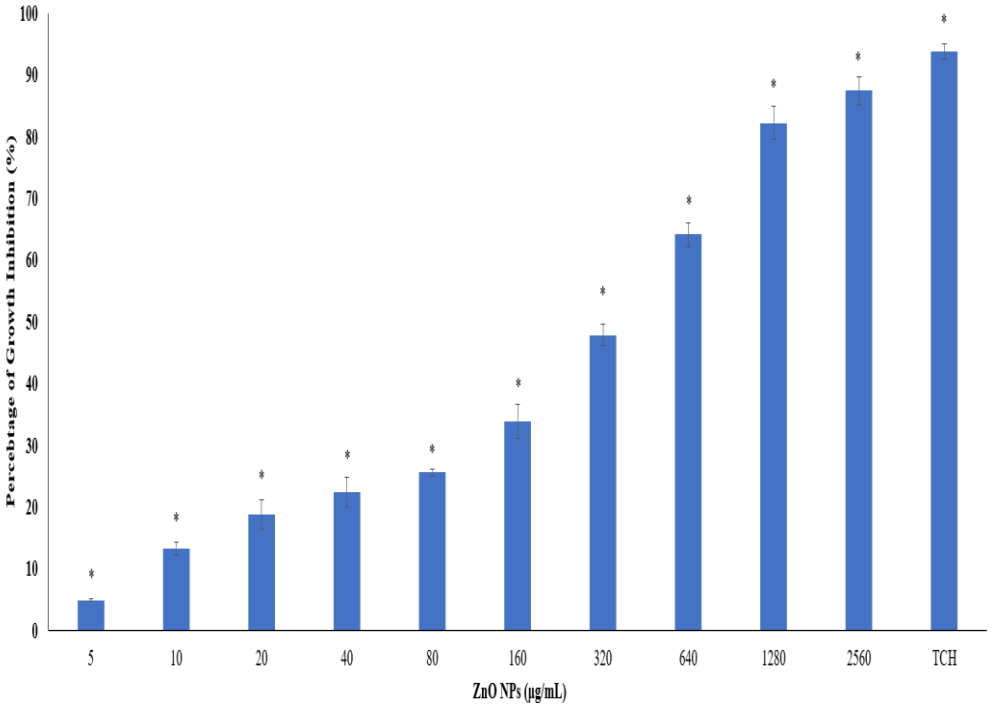

Figure 4.5: The growth inhibition percentage of *K. pneumoniae* treated by different ZnO NP concentrations and the positive control for 24 h at 37°C in TSB obtained from the turbidity method. The values plotted in the graph are in mean ± standard deviation.

* Indicates the significance difference between the growth inhibition percentage between the negative control and the ZnO NP treated bacterial suspension ($p < 0.05$).

4.5.2 INT Assay

INT assay was used to identify the MIC of ZnO NPs that can inhibit the visible growth of *K. pneumoniae* by observing the appearance of colour formation for each bacterial suspension that was treated with different ZnO NP concentrations (5, 10, 20, 40, 80, 160, 320, 640, 1280, and 2560 μg/mL). Based on **Figure 4.6**, no colour formation was observed for columns K and L as well as nanoparticle controls for the three sets of data after being incubated with INT dye for 20 mins.

Table 4.4 and **Figure 4.7** depict the growth inhibition of *K. pneumoniae* after 24 h incubation. The results showed statistically significant (p <0.05) *K. pneumoniae* growth inhibition by all the tested ZnO NP concentrations at 24 h as compared to the negative control, with the resultant values of 5.47 ± 0.76, 12.06 ± 1.07, 16.20 ± 2.29, 22.97 ± 1.36, 31.92 ± 1.18, 38.49 ± 2.33, 44.58 ± 2.24, 65.82 ± 0.96, 83.55 ± 1.23, and 87.29 ± 0.74% for 5, 10, 20, 40, 80, 160, 320, 640, 1280, and 2560 μg/ mL of ZnO NPs, respectively.

(a)

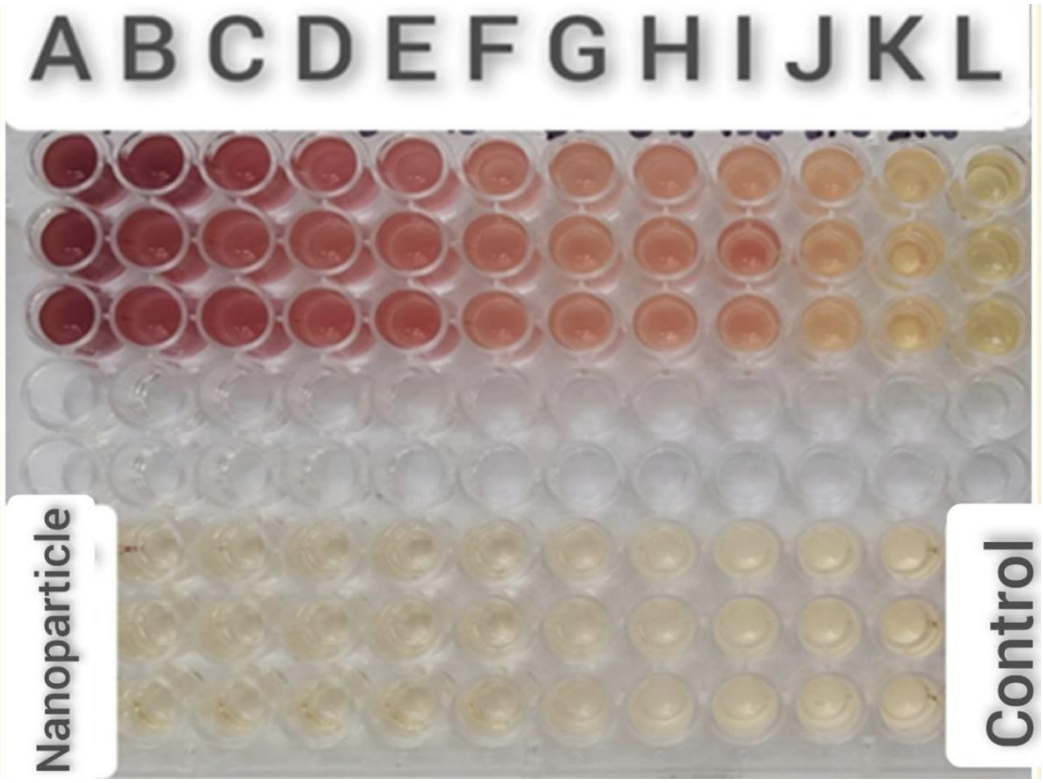

(b)

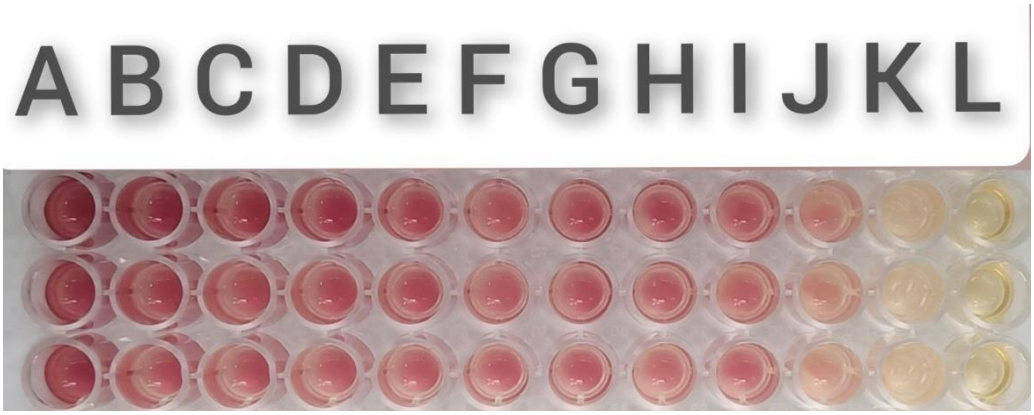

(c)

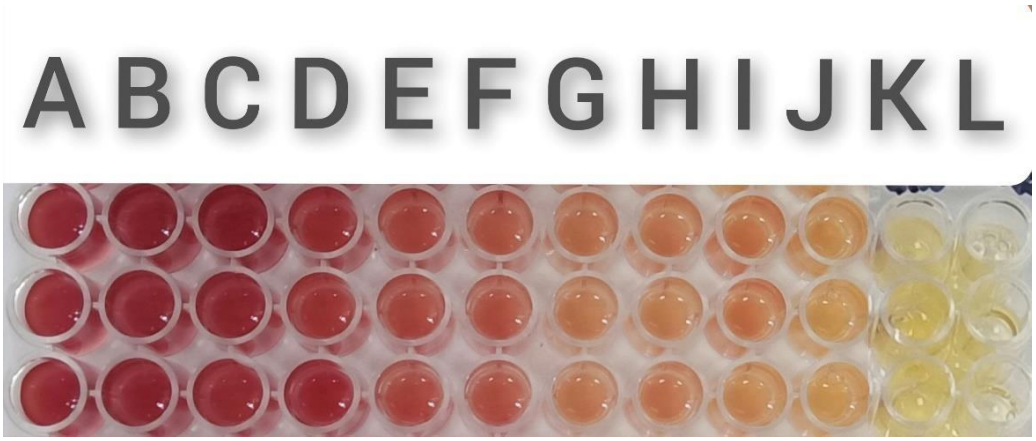

Figure 4.6: The colour changes of *K. pneumoniae* after treated with **(B)** 5 µg/mL; **(C)** 10 µg/mL; **(D)** 20 µg/mL; **(E)** 40 µg/mL; **(F)** 80 µg/mL; **(G)** 160 µg/mL, **(H)** 320 µg/mL, **(I)** 640 µg/mL, **(J)** 1280 µg/mL, **(K)** 2560 µg/mL of ZnO NPs as compared to negative control **(A)** and positive control **(L)**.

Table 4.4: The growth inhibition percentage of *K. pneumoniae* treated by different ZnO NP concentrations and the positive control for 24 h at 37°C in TSB obtained from the INT assay.

ZnO NP concentration (µg/mL)	Percentage of growth inhibition (%)
5	5.47 ± 0.76
10	12.06 ± 1.07
20	16.20 ± 2.29
40	22.97 ± 1.36
80	31.92 ± 1.18
160	38.49 ± 2.33
320	44.58 ± 2.24
640	65.82 ± 0.96
1280	83.55 ± 1.23
2560	87.29 ± 0.74
TCH (1 mg/mL)	92.97 ± 1.18

Mean ± Standard deviation, n=3

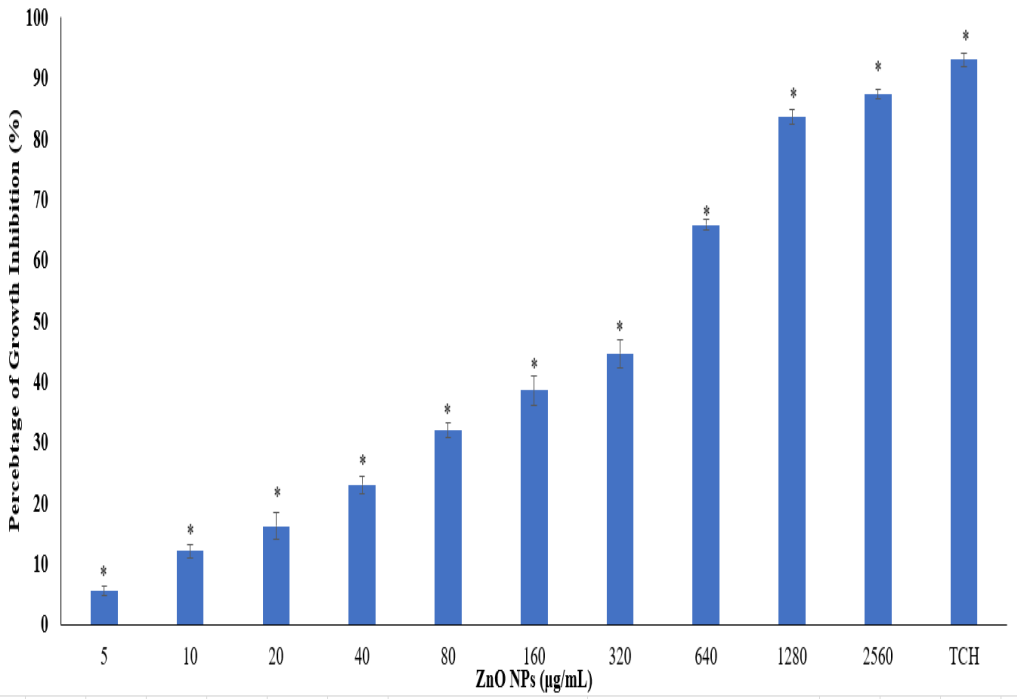

Figure 4.7: The growth inhibition percentage of *K. pneumoniae* treated by different ZnO NP concentrations and the positive control for 24 h at 37°C in TSB obtained from the INT assay. The values plotted in the graph are in mean ± standard deviation.

* Indicates the significance difference between the growth inhibition percentage between the negative control and the ZnO NP treated bacterial suspension ($p < 0.05$).

4.5.3 Minimum Bactericidal Concentration (MBC) Assay

By referring to the MIC result, only solution that remained a yellowish colour in the well after INT addition was pipetted into TSA plates for MBC assay. Therefore, the MBC value determination was done by observing the presence of bacteria colonies growing on the TSA plate. The lowest concentration of ZnO NPs that showed no colony growth was considered as the MBC value. As shown in **Figure 4.8**, *K. pneumoniae* treated with 2560 µg/mL of ZnO NP formed eight colonies.

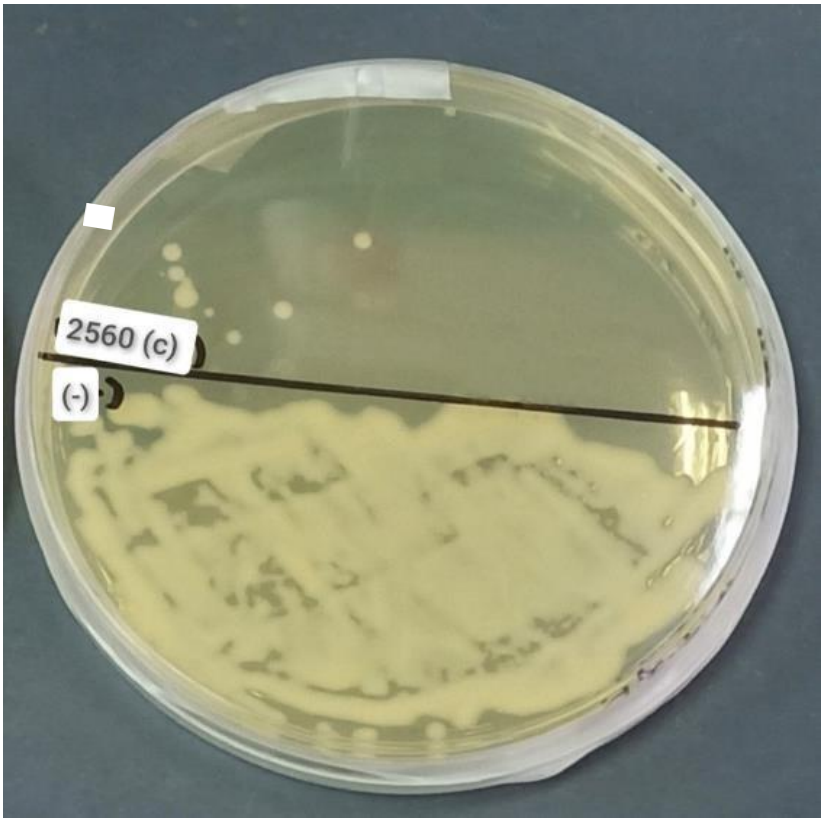

Figure 4.8: Colonies of *K. pneumoniae* formed on TSA at 37 °C for 24 h in the negative control **(-)** and *K. pneumoniae* suspension exposed to 2560 µg/mL of ZnO NPs **2560**.

4.6 Surface Interaction and Cellular Accumulation of ZnO NPs on Bacteria

4.6.1 Fourier Transform Infrared (FTIR) Spectroscopy

FTIR analysis helped identify *K. pneumoniae* surface functional groups that might involve in ZnO NP attachment. As shown in **Figure 4.9**, the peak shifting between the negative control and 2560 µg/mL ZnO NP treated bacterial suspension for 24 h were compared and analysed. The bacterial surface functional groups possibly involved in interacting with ZnO NPs was tabulated in **Table 4.5.** According to **Figure 4.9 (a)** the spectrum obtained for the negative control demonstrated N-H and O-H stretching at 3297 cm^{-1}, C-H stretching at 2925 cm^{-1}, C≡C stretching at 2108 cm^{-1}, NH_2 bending, C=O and C–N stretching polypeptide and protein backbone at 1656 cm^{-1}, N–H bending and C–N stretching at 1541 cm^{-1}, CH_2 bending of lipids at 1454 cm^{-1}, –COO− at 1398 cm^{-1}, PO_2^- asymmetric stretching at 1238 cm^{-1}, PO_2^- symmetric stretching and C-O stretching at 1082 cm^{-1}, C–N^+–C stretching of nucleic acids at 967 cm^{-1}, polysaccharides and glycosidic linkages at 967 and 934 cm^{-1}, C—H stretching, N-type sugar; coupled furanose–phosphodiester chain, and polysaccharides within the cell wall at 860 cm^{-1}, and glycogen at 542 cm^{-1}.

On the other hand, **Figure 4.9 (b)** depicts that the peaks that shifted in 2560 µg/mL ZnO NPs treated bacteria for 24 h were N-H and O-H stretching (3297 to 3375 cm^{-1}), C≡C stretching (2108 to 2102 cm^{-1}), NH_2 bending, C=O and C–N stretching (1656 to 1651 cm^{-1}), N–H bending and C–N stretching (1541 to 1528 cm^{-1}), PO_2^- symmetric stretching and C-O stretching to C—C/ C—O/ O—H stretching (1082 → 1027 cm^{-1}), C—H stretching (860 to 830 cm^{-1}), and

Zn-O stretching (542 to 562 cm^{-1}). Herein, surface functional groups such as alcohol and amide A (3375 cm^{-1}), alkynes (2102 cm^{-1}), amide I (1651 cm^{-1}), amide II (1528 cm^{-1}), phosphate group (1082 cm^{-1}), aliphatic group (1027 cm^{-1}), amine group (830 cm^{-1}) from the cell wall of *K. pneumoniae* may be involved in the interaction with ZnO NPs.

The peaks found at 2925, 967, and 934 cm^{-1} in the control were missing in the treated sample. Besides, peaks at 781 and 541 cm^{-1} were newly formed in the test peaks representing Zn-O stretching.

.

(a)

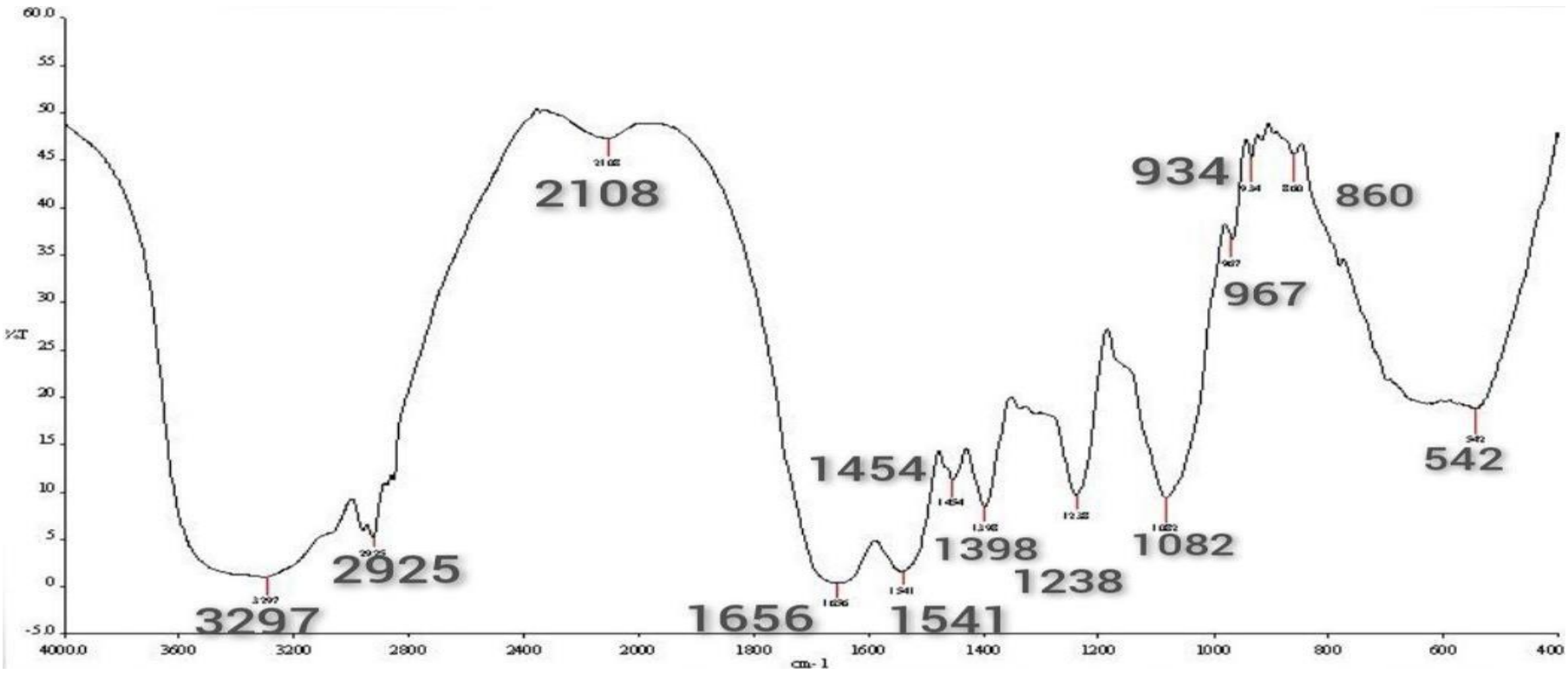
3297
2925
2108
1656
1541
1454
1398
1238
1082
967
934
860
542
%T
cm-1

(b)

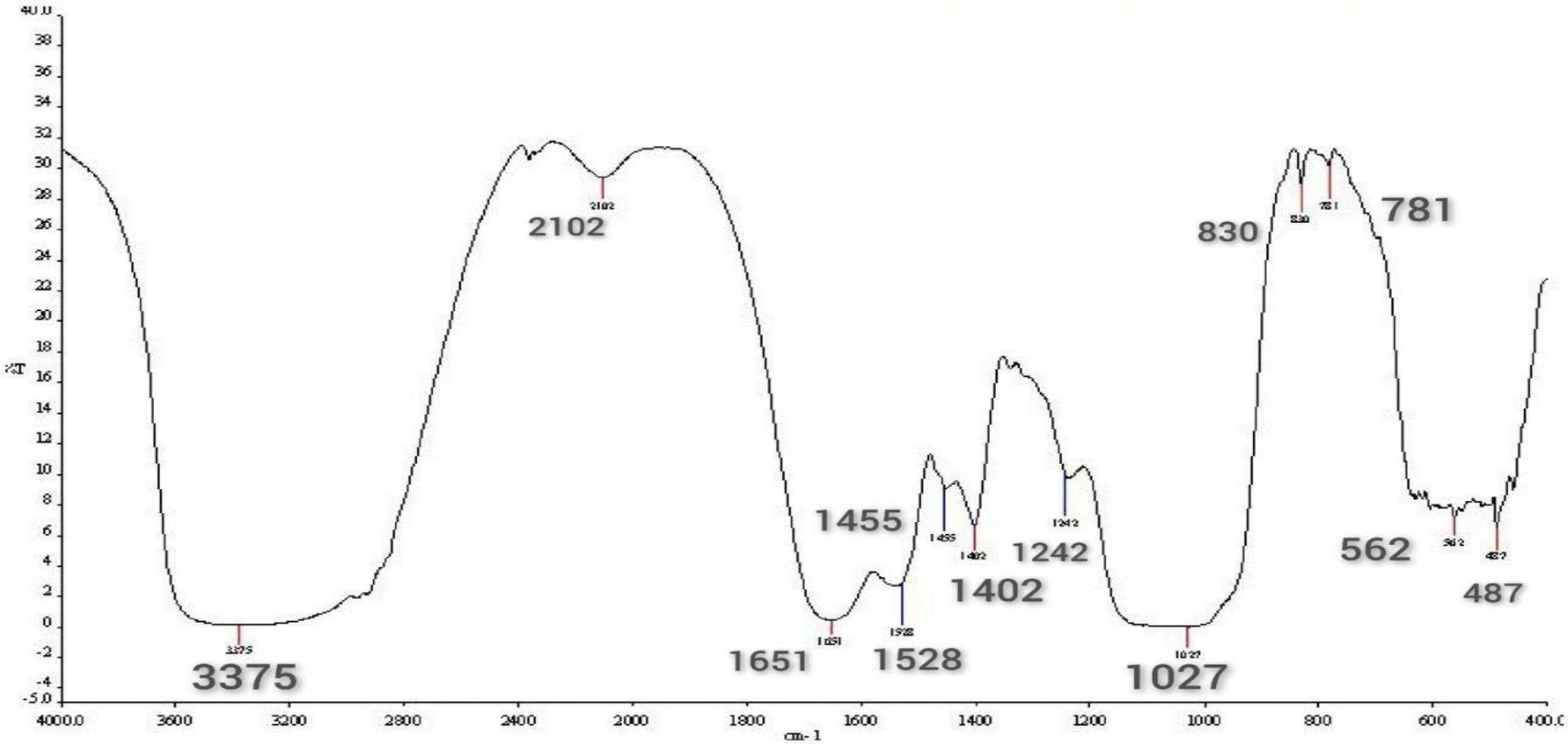

Figure 4.9: FTIR spectrum of **(A)** untreated control, **(B)** 2560 µg/mL ZnO NPs treated *K. pneumoniae.*

Table 4.5: Possible bacterial functional groups involved in the interaction with ZnO NPs in FTIR analysis.

Absorption (cm^{-1})	Molecular motion	Functional group	Biomolecules
3297 → 3375	O–H and N–H stretching	Amide A, alcohol	Polysaccharides, proteins, intermolecular hydrogen bond
2108 → 2102	C≡C stretching	Terminal alkyne	Hydrocarbon
1656 → 1651	NH_2 bending, C=O and C–N stretching	Amide I	Polypeptide, protein backbone (α helices)
1541→ 1528	N–H bending, C–N stretching	Amide II	protein (α helices)
1082 → 1027	PO_2^- symmetric stretching and C-O stretching → C—C/ C—O/ O—H stretching	Phosphate group, aliphatic group	nucleic acids and phospholipids (PO_2^- symmetric stretching), and glycogen (C-O stretching) → Polysaccharides
860→ 830	C—N stretching	Amine group	Polysaccharides, protein
542→ 562	Zn-O stretching	Zinc oxide	Glycogen

4.6.2 Energy Dispersive X-ray (EDX) Analysis

The cellular accumulation of ZnO NPs on *K. pneumoniae* was analysed by EDX analysis. According to **Figure 4.10**, the EDX spectrum depicts that carbon (C), oxygen (O), sodium (Na), phosphorus (P), chlorine (Cl), and potassium (K) were present in the negative control sample. On the other hand,

Figure 4.11 illustrates the presence of zinc (Zn) after 24 h treatment of *K. pneumoniae* with 2560 µg/mL of ZnO NPs compared to the negative control.

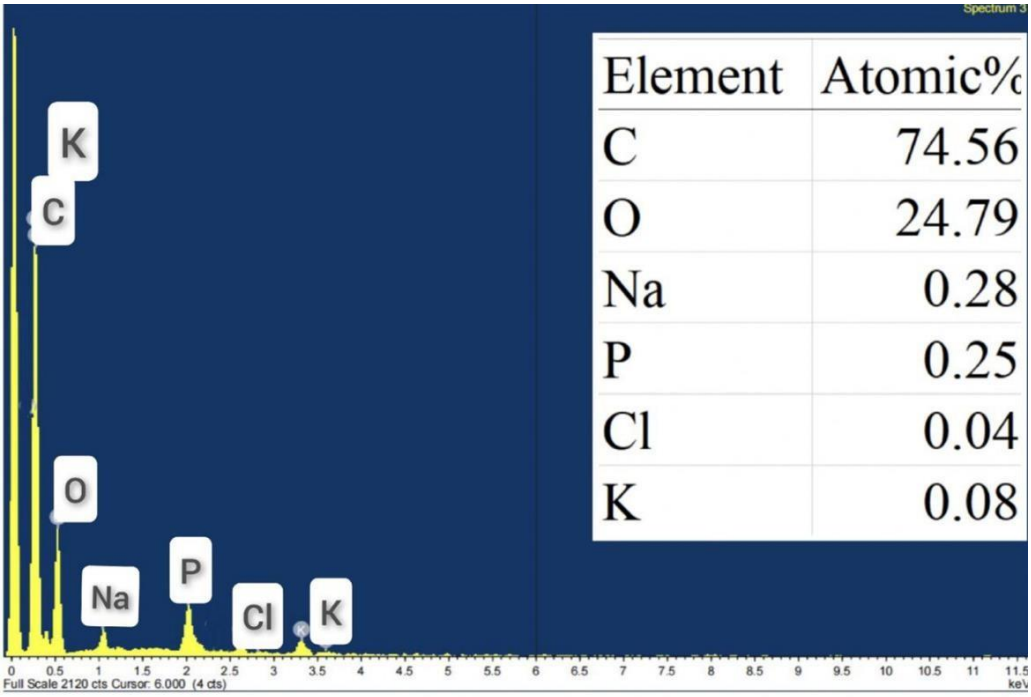

Figure 4.10: EDX spectrum depicts that carbon, oxygen, sodium, phosphorus, chlorine, and potassium were present in the negative control.

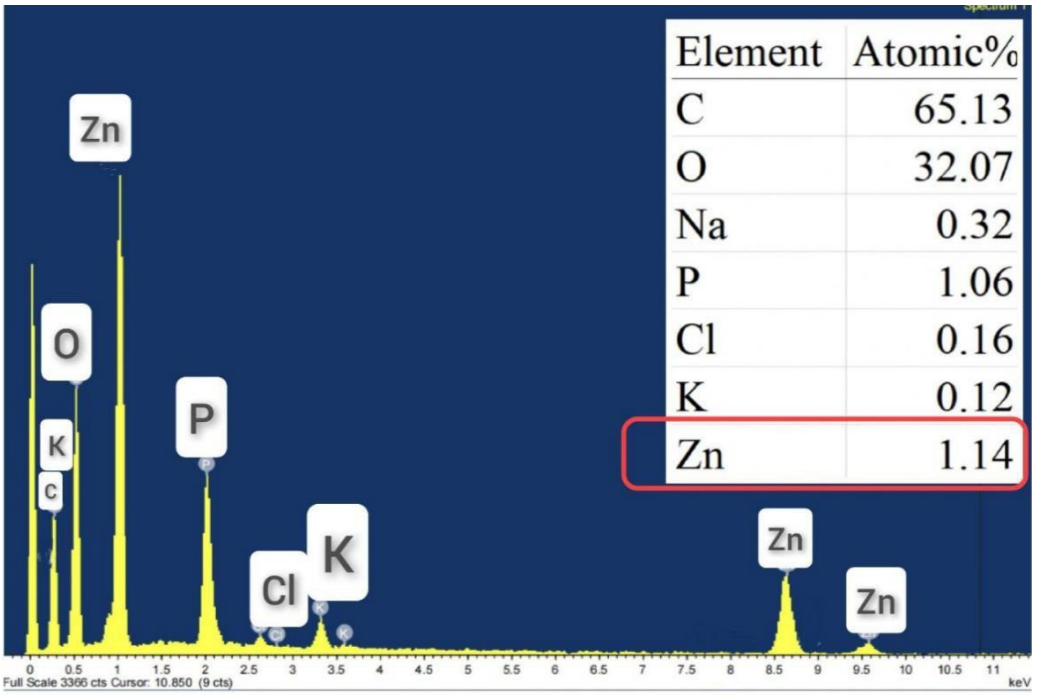

Figure 4.11: EDX spectrum of 2560 µg/mL ZnO NPs treated *K. pneumoniae* shows the agglomeration of ZnO NPs on the bacterial cell surface.

4.7 Scanning Electron Microscope (SEM) Analysis

Scanning electron microscope was used to study the morphological changes of *K. pneumoniae* upon treating with 2560 µg/mL of ZnO NPs. **Figure 4.12 (A)** is the image of negative control under 15, 000× magnification and scale bars are in 1 µm. The negative control demonstrated smooth cell surface, intact and uncompromised cell membrane. Alterations in cell structure can be observed after the treatment of *K. pneumoniae* with 2560 µg/mL of ZnO NPs at 24 h. Based on **Figure 4.12 (B), (C), (D), (E)** and **(F)**, the harvested bacterial suspension showed aggregation of bacterial cells, roughening of cell surface, shrinkage of bacteria cells, ZnO NP aggregation on cell membrane, membrane damage, cell distortion, and rupture of cell membrane.

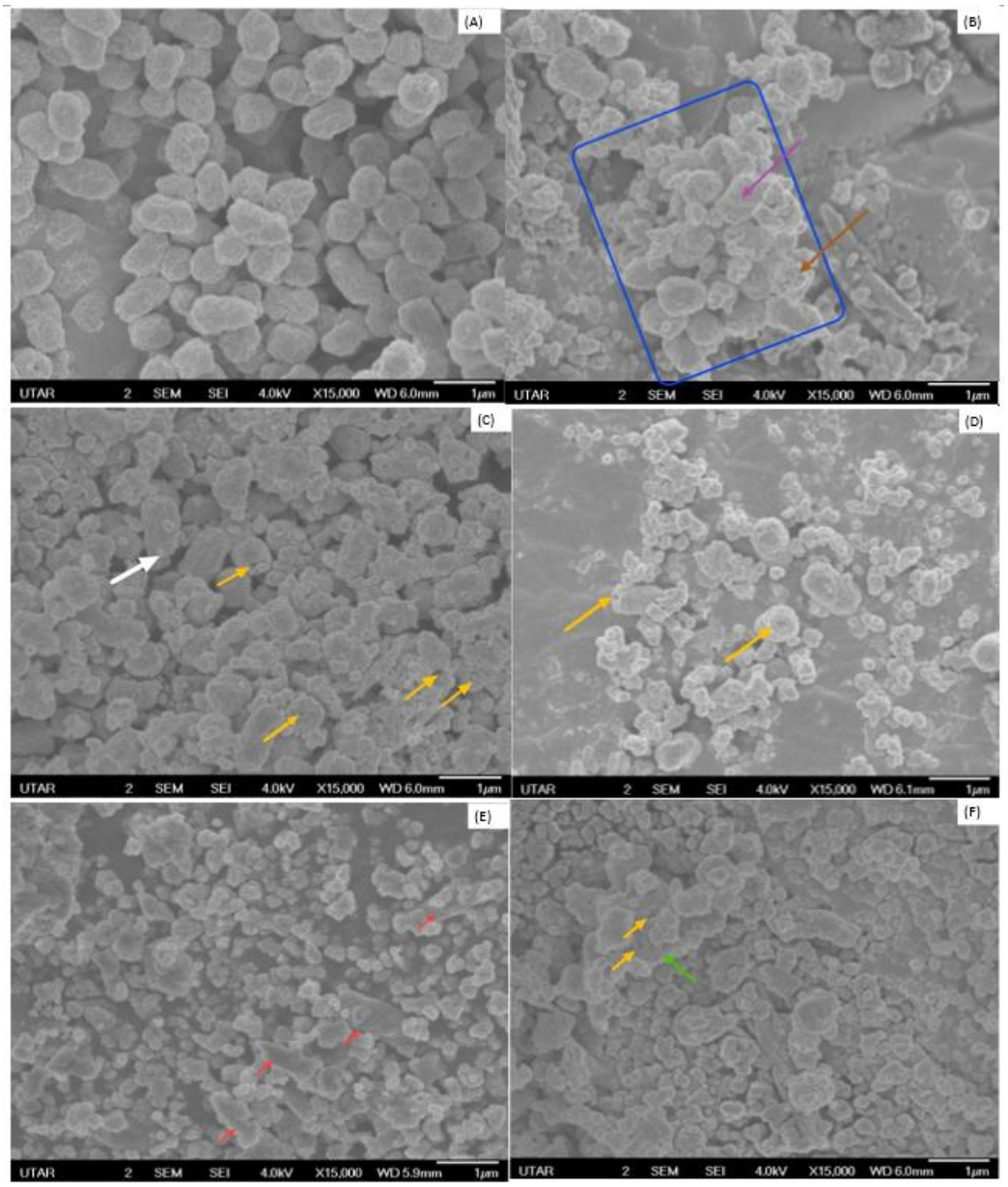

Figure 4.12 SEM micrographs of *K. pneumoniae* control (**A**) and *K. pneumoniae* exposed to 2560 µg/mL ZnO NPs for 24 h illustrating bacterial cell aggregation (blue box), roughening of cell surface (purple arrow), and shrinkage of bacteria cells (brown arrow) (**B**), ZnO NP aggregation on cell membrane (white arrow) (**C**), membrane damage (yellow arrow) (**C**, **D**, and **F**), cell distortion (red arrow) (**E**), and rupture of cell membrane (green arrow) (**F**).

CHAPTER 5

DISCUSSION

5.1 ZnO NP Characterization

Shapes and sizes of ZnO NPs being observed from SEM analysis were spherical, mixed with rod shapes, and 86.8 nm, respectively. The presence of only zinc, oxygen, and carbon peaks in EDX spectrum indicated the high purity of ZnO NPs used in the present study. Presence of carbon may be due to the use of carbon tape for SEM analysis (Fakhari et al., 2019; Osuntokun et al., 2019; Varadavenkatesan et al., 2019).

5.2 Growth Inhibition Tests

The ZnO NP growth inhibitory effects on *K. pneumoniae* were assessed by the turbidity method and INT assay to evaluate the bacteriostatic effects of ZnO NPs. The following streak plate method functioned to determine the MBC. The present study results showed that the growth inhibition of *K. pneumoniae* treated with 5, 10, 20, 40, 80, 160, 320, 640, 1280, and 2560 μg/mL ZnO NPs increased from 5, 13, 19, 22, 26, 34, 48, 64, 82 to 87%, respectively at 24 h. The percentage of *K. pneumoniae* growth inhibition obtained from the INT assay supported the turbidity assay results, showing 5,

12, 16, 23, 32, 38, 45, 66, 84, 87% with the corresponding ZnO NP concentrations. Compared to the negative control, all tested ZnO NP concentrations showed significantly different growth inhibition activity against *K. pneumoniae*. Therefore, the alternative hypothesis was accepted. The increase in turbidity results from serial dilutions of ZnO NPs, indicating bacterial growth. Therefore, higher NP concentrations had greater antimicrobial effects.

The MIC is the lowest antimicrobial concentration that can inhibit the growth of microbes, while MBC is the lowest antibacterial concentration that can kill 99.9% of bacteria (Pelletier and Baker, 1988). The lower the MIC value, the more effective the antimicrobial agent. The microbroth dilution susceptibility method in 96-well microtiter plates is preferred for antimicrobial susceptibility testing because it has few sample requirements, is cost-effective, and has a high throughput rate (Coutinho et al., 2010). The p-Iodonitrotetrazolium chloride (INT) assay is a microplate assay that determines the MIC of antimicrobials using INT dye. The enzymatic reaction of viable microorganisms will reduce the yellow tetrazolium dye, which acts as an electron acceptor, into a pink product, the insoluble iodonitrotetrazolium formazan or INF (Li et al., 2010). The MIC for the INT assay is the lowest antimicrobial concentration that completely inhibits bacterial growth and prevents the appearance of a pink dye (Ríos and Recio, 2005). The absence of colonies on the streak plate reveals MBC at this antimicrobial concentration.

In this study, no colour changes were observed in the wells for 2560 µg/mL of ZnO NPs, indicating that the MIC value of ZnO against *K. pneumoniae* was 2560 µg/mL, that can inhibit the visible growth of *K. pneumoniae* after overnight incubation. No colour change was observed in wells containing sterility controls, depicting that ZnO NPs were not contaminated. Colony formation obtained from the MBC assay indicated that 2560 µg/mL of ZnO NPs cannot kill 99.9% of the bacteria. Therefore, 2560 µg/mL of ZnO NPs was considered as the MIC but not the MBC for *K. pneumoniae*. The MBC value was predicted to be higher than 2560 µg/mL of ZnO NPs as 99.9% of bacteria inhibition had not yet been achieved.

Numerous previous studies have reported a similar finding to the present study on *K. pneumoniae* growth inhibition by ZnO NPs. Like our methods, Shivaee et al. (2021) prepared turbidity of microbial broth with 0.5 McFarland standard and incubated a 96-well plate at 37 ºC for 24 h. They determined the MIC of ZnO NPs using the microdilution method to be 2500 µg/ml against all five *K. pneumoniae* isolates. Hameed et al. (2016) reported a dose-dependent growth inhibition from 0.32, 4.91, 7.92, 17.43, 25.20, 38.99, 58.48, 77.5, to 89.7% for 50, 150, 250, 350, 500, 650, 800, and 1000 µg/mL of ZnO NPs respectively, in comparison with the negative control. In a research conducted by Nazoori and Kariminik (2018), the MBC of ZnO NPs was reported to be 10000 µg/mL, which is higher than 2560 µg/mL.

A study done by Imade et al. (2022) showed 0.00, 15.51, 29.71, 31.76, and 34.86% of inhibition for 10, 100, 500, 1000, and 5000 μg/ml of ZnO NP synthesised using plantain peel extract (PPE), respectively at 24 h. The turbidity of *K. pneumoniae* suspension exposed to 5000 μg/mL of ZnO NPs decreased to about 65% at 24 h of incubation compared to the negative control at an optical density of 600 nm. However, the MIC for the NPs was determined to be 100 μg/mL with a 15.51% percentage of inhibition for *K. pneumoniae*. The promising antibacterial activities of ZnO NP reported might be due to the small particle size of 12.45 nm and its spherical morphology due to green synthesis using PPE. On the other hand, the NPs in our study have a mean dimension of 86.8 nm and consist of spheres and rods. A smaller particle has a higher solubility and thus better dissolution into Zn^{2+} ions to inhibit bacteria (Webster and Seil, 2012). Moreover, the smaller size enables easier penetration through the bacterial cell, and the results are membrane leakage and cell death (Vielkind et al., 2013).

The typical dose-dependent antibacterial activities were reported in other studies using other methods. Ansari et al. (2011) reported that 1000 μg/ml of ZnO NPs could achieve 98.6% inhibition in the colony-forming ability of *K. pneumoniae*. Obeizi et al. (2020) synthesized ZnO NPs from *Eucalyptus globulus* essential oil and determined the MIC value for *K. pneumoniae* to be 16 μg/mL. In their study, the zone of inhibition (ZI) for 25, 50, 75, 100 μg/ml of ZnO NPs were 15.41 ± 0.24, 17.27 ± 0.53, 18.63 ± 0.27, and 19.35 ± 0.45 mm, respectively. By incubating *K. pneumoniae* with ZnO NPs in nutrient

broth for 14 h at 37°C, the MIC of ZnO NPs synthesised by Reddy et al. (2014) from the precipitation method was found to be 40 µg/mL. In a study conducted by Sharma et al. (2019), the increase in ZnO NP concentrations from 25, 50, 100, to 200 µg/mL enhances its inhibitory activity against *K. pneumoniae*, as shown by the ZI of 19, 20, 22, and 25 mm, respectively. Their ZnO NPs possess maximum inhibitory activity against *K. pneumoniae* followed by *Salmonella typhi*, *Escherichia coli*, *Staphylococcus aureus*, and *Pseudomonas aeruginosa.* We study the antibacterial properties of ZnO NPs with the microbroth dilution method using tryptic soy broth (TSB). According to Schuurmans et al. (2009), different protocols may contribute to different MIC values that were identified through different growth inhibitory tests, although the same antimicrobial compound and bacteria were used. Growth medium compositions and physicochemical parameters can also influence growth conditions (Raghupathi et al., 2011; Shankar and Rhim, 2019).

Although they are generally less potent, green synthesised NPs using plant extracts are gaining more attention as they are considered less toxic compared to synthetic NPs (James and Cohen, 1980; Rajakumar et al., 2012). With *K. pneumoniae* (ATCC700603) as a control, Rasha et al. (2021) tested the effects of ZnO NPs synthesised using *Aspergillus niger* on carbapenemase-producing strains of *K. pneumoniae* (KPC). All tested bacteria and the control were highly sensitive to the synthesised ZnO NPs, with a mean score of 700 and 1800 µg/ml, for MIC and MBC, respectively, in all tested KPC. In a similar study,

the researchers synthesised ZnO NPs using *Acacia nilotica* and obtained a mean score of 450 and 1140 µg/ml for MIC and MBC, respectively (Rasha et al., 2021b). However, the relatively high bacterial titer used in this research may result in an inoculum effect (IE) that is associated with a significant increase in the MIC of ZnO NPs (Smith and Kirby, 2018) even though we used synthetic ZnO NPs. Our study may provide an insight into the efficacy of ZnO NPs against high bacterial titer.

In a study conducted by Venkatasubbu et al. (2016), which used ZnO and titanium dioxide (TiO_2) NPs for *Salmonella typhi*, *K. pneumoniae*, and *S. flexneri*, the MIC_{50} of ZnO NPs was shown to be lower than TiO_2 NPs, indicating that lower concentration of ZnO NPs was needed to inhibit 50% of the bacterial growth as compared to TiO_2 NPs. However, the inhibition percentages of 5, 10, 20, 40, and 80 µg/ml of TiO_2 NPs reported by Anbumani et al., (2022) against *K. pneumoniae* using the microbroth dilution method were gradually higher than our results. The degree of susceptibility and tolerance of different bacterial strains to antibacterial agents may vary based on metal nanoparticles (MNPs).

Several mechanisms were proposed for the bacterial growth inhibition by ZnO NPs: bactericidal effects due to the hydrogen peroxide production on the bacterial surface (Siddique et al., 2013; Mostafa, 2015; Prakash and Kalyanasundharam, 2015; Pandimurugan and Thambidurai, 2017); loss in cell

membrane integrity due to the agglomeration of NPs on the bacterial surface and ROS production (Soren et al., 2018; Husen, 2019); and internalization of ZnO NPs into bacteria cells and the release of Zn^{2+} ions (Soren et al., 2018).

5.3 Surface Interaction and Cellular Accumulation of ZnO NPs

The interaction of ZnO NPs with *K. pneumoniae* cell envelope was analysed by the FTIR spectroscopy to identify nacterial cell surface functional groups involved in contacting with ZnO NPs. The functional group concentration can be determined from the total band area, while the conformational freedom and flexibility can be predicted from the bandwidth (Kardas et al., 2014). The FTIR spectrum of ZnO NPs treated *K. pneumoniae* illustrated the possible involvement of amine, hydroxyl, carbonyl, phosphate, and aliphatic groups of polysaccharides, proteins, glycogen, and phospholipids from *K. pneumoniae* cell envelope in interacting with ZnO NPs.

The N-H and O-H group stretching vibration from the polysaccharides, proteins, and intermolecular hydrogen bond dominate the region between 3375 and 3297 cm^{-1} (Melin et al., 2000; Naumann, 2001; Gorgulu et al., 2007). According to Ifeanyichukwu et al. (2020), the bacterial cell surface hydroxyl group can bind to Zn^{2+} ions. The region between 2108 and 2102 cm^{-1} was belong to the C≡C stretching vibration in the terminal alkyne (Thomas et al., 2014; Peng et al., 2018; Nandiyanto et al., 2019).

The region between 1656 and 1651 cm^{-1} was the conformation-sensitive amide I band of β-pleated sheet structures, predominantly attributed to C=O stretching in polypeptides and protein backbone, α-helical structure (Melin et al., 2000; Naumann, 2001; Gorgulu et al., 2007; Wang et al., 2012; Bhat, 2013; Maity et al., 2013). As the vibration frequency in the amide I region is highly sensitive to hydrogen bond changes in different protein secondary structures, this region is vital to predicting the secondary structure of a protein (Gorgulu et al., 2007). The strong protein amide I bands usually overlapped the weak nucleic acid between the region (Naumann, 2001). Absorption of Amide II at 1541 and 1528 cm^{-1} primarily involves an N–H bending coupled to a C–N stretching vibrational mode (Wood et al., 1998; Huang et al., 2003). This peak shifting suggested protein degradation in treated *K. pneumoniae* (Burattini et al., 2008).

The PO_2^- symmetric stretching of nucleic acids and phospholipids; and C-O stretching of glycogen can be found between 1082 and 1027 cm^{-1} (Melin et al., 2000; Gorgulu et al., 2007; Wang et al., 2012). Sugar, lipid, and protein constitute Gram-negative bacteria cell walls. Production of ROS will cause membrane lipid peroxidation, cellular sugar and protein leakage, and eventually apoptosis. According to Dadi et al. (2019), the interaction between ZnO NPs and Gram-negative bacteria results in progressive leakage of lipopolysaccharides from their cell walls and cell lysis. Absorption peaks at 860 and 830 cm^{-1} involve C—N stretching of the amine group in polysaccharides and proteins (Gupta et al., 2018).

Three peaks were only found in the control but not the the treated sample: 2925, 967, and 934 cm^{-1}, indicating the possible masking of the existing functional groups due to the NP accumulation on the bacterial cell envelope. The peak found at 2925 cm^{-1} was contributed by CH_2 asymmetric stretching that is predominantly lipids with a minor contribution from proteins, carbohydrates, and nucleic acids (Gorgulu et al., 2007); 967 and 934 cm^{-1} refer to polysaccharides and glycosidic linkages (Bhat, 2013).

The newly formed peak at 781 and 487 cm^{-1} in ZnO NPs treated sample represents the Zn-O stretching (Shahvalizadeh et al., 2021). Glycogen (Bhat, 2013) and Zn-O bonds (Shahvalizadeh et al., 2021) contributed peaks between 542 and 562 cm^{-1}.

Previous research suggested that bacterial cell surface functional groups, such as carboxyl, hydroxyl, and amine groups, were predicted to bind with Zn^{2+} ions (Yusof et al., 2020). This statement was compatible with the present FTIR analysis. Moreover, the results obtained agreed with previous studies that involve various organisms. For example, the interaction of Gram-negative bacteria *Pseudomonas putida* with Hematite-coated germanium crystal was found to involve hydroxyl, carbonyl, amino, and aliphatic groups of polysaccharides, proteins, and lipids. Besides, Djearamane et al. (2018) and Liang et al. (2020) reported the involvement of hydroxyl, carboxyl, and amino groups in polysaccharides, glycogen, and proteins when ZnO NPs were used to

treat the algae, *Spirulina platensis*, and Gram-positive bacteria, *Streptococcus pyogenes*, respectively.

Furthermore, the EDX analysis was performed to determine the elemental composition of chemicals present on the bacterial cell membranes and confirm the cellular accumulation of ZnO NPs onto *K. pneumoniae*. X-ray was formed owning to the energy differences when the hole in the lower energy shell was filled by the electron from the higher electron shell. Each element has a unique atomic number that can identify by the X-ray (Nanakoudis, 2019). As shown in **Figure 4.5**, no peaks were visible for zinc (Zn) in the EDX spectrum of the negative control. On the contrary, **Figure 4.6** showed the significant peaks representative of Zn, confirming the presence of Zn in the bacterial cell after being exposed to 2560 μg/mL of ZnO NPs. Similar findings were obtained by Djearamane et al. (2018) in algal biomass after 96 h of treatment with 200 μg/mL of ZnO NPs. Likewise, Liang et al. (2020) observed a five-fold increase in Zn levels in the EDX spectrum of *Streptococcus pyogenes* exposed to 100 μg/mL of ZnO NPs for 24 h.

An increased atomic percentage of Zn after the exposure of *K. pneumoniae* to ZnO NPs confirmed ZnO NP accumulation on the treated bacterial cell surface (Liang et al., 2020). Besides, sodium (Na), phosphorus (P), chlorine (Cl), and potassium (K) were found in both the negative control sample and *K. pneumoniae* sample that was exposed to ZnO NPs, as these elements could be

found in the growth medium (tryptic soy broth). In addition, P also presents in the phosphate buffer saline (PBS) involved in the sample processing (Liang et al., 2020).

The agglomeration of ZnO NPs onto *K. pneumoniae* might be resulted from the electrostatic attraction between the cationic Zn^{2+} ions and anionic functional groups on bacteria (Huang et al., 2015). The subsequent specific interactions will disrupt the function of these groups (Reddy et al., 2014), causing a change in membrane potential. Therefore, membrane depolarization leads to membrane integrity loss (Zhang et al., 2010; Shilpi et al., 2014). The Zn^{2+} ions are the main contributor to the antibacterial effects of ZnO NPs (Sirelkhatim et al., 2015; Mohd Yusof et al., 2019). The dissolution of attached ZnO releases Zn^{2+} ions that could penetrate through microbial cell walls. In the cytosol, Zn^{2+} ions bind with sulphur-containing amino acids, interfere with the bio-signalling, inactivate the electron transport chain, and reduce ATP production, causing mitochondrial oxidative stress (Kasi et al., 2019). The toxic Zn^{2+} ions also cause membrane leakage and loss of proton motive force (Patra et al., 2017).

5.4 Morphological Changes of Bacteria

Morphological alterations were observed after the exposure of *K. pneumoniae* to 2560 µg/mL of ZnO NPs. For the negative control sample, bacterial cells conserved the intact cell wall. However, after the exposure to ZnO NPs, *K. pneumoniae* showed aggregation of bacterial cells, roughening of cell surface,

shrinkage of bacteria cells, adsorption of ZnO NPs on cell membrane, membrane damage, cell distortion, and rupture of cell membrane. **Figure 5.1** is a schematic illustration depicting toxicity mechanism of ZnO NPs.

Bacterial cell aggregation could have resulted from the self-defense mechanism of bacterial cells. For instance, exopolysaccharide (EPS) secretion from stressed cells increases cell-cell interaction (Sadiq et al., 2011) and thus, reduces the surface area of bacterial cells available for ZnO NP binding. The ZnO NPs interact with bacterial membrane biomolecules to accumulate on cell surface and induce ROS overproduction (Chen et al., 2012).

The small size of ZnO NPs enables them to enter bacterial cells, thereby intensifying their bactericidal activity (Sirelkhatim et al., 2015). The ROS generated by ZnO NPs like hydrogen peroxide (H_2O_2), peroxide ion (O_2^{2-}), hydroxyl radical (OH^-), superoxide (O_2^-), and singlet oxygen (Tayel et al., 2011; Paisoonin et al., 2013) will inactivate respiratory enzymes, break down cell walls, and increase membrane permeability with the exertion of mechanical stress. The oxidative stress damage leads to the leakage of cell contents and facilitates ZnO NP entrance and zinc ion (Zn^{2+}) uptake, which will produce more ROS in the cytoplasm (Brayner et al., 2006). The reaction of Zn^{2+} ions with cytoplasmic components and the overproduced ROSs impair bacterial metabolism by causing the attenuation of DNA replication and dysfunctional adenosine triphosphate (ATP) synthesis, inhibiting bacterial growth or even

lysing, and killing them (Li et al., 2011; Sharma and Chaudhary, 2020). Ultimately, mitochondrial dysfunction, cytoplasmic leakage, and oxidative stress lead to membrane damage and bacterial death (Hu et al., 2019; Tang et al., 2019).

The results agreed with previous studies done on ESBL-producing *K. pneumoniae* (Hameed et al., 2016), *Bacillus cereus* (Aguilar et al., 2015), *Bacillus licheniformis* (Dalai et al., 2012), *Campylobacter jejuni* (Siddiqi et al., 2018), *Chlorella vulgaris* (Djearamane et al., 2019), *Pseudomonas aeruginosa (*Dhanasegaran et al., 2021), *Escherichia coli* (Zhang et al., 2008; Arakha et al., 2015), after exposing to Neodymium (Nd) doped ZnO NPs, organic NPs with silver/gold (Ag/Au) NPs, titanium dioxide (TiO_2) NPs, ZnO NPs, and iron oxide (Fe_2O_3) NPs, respectively.

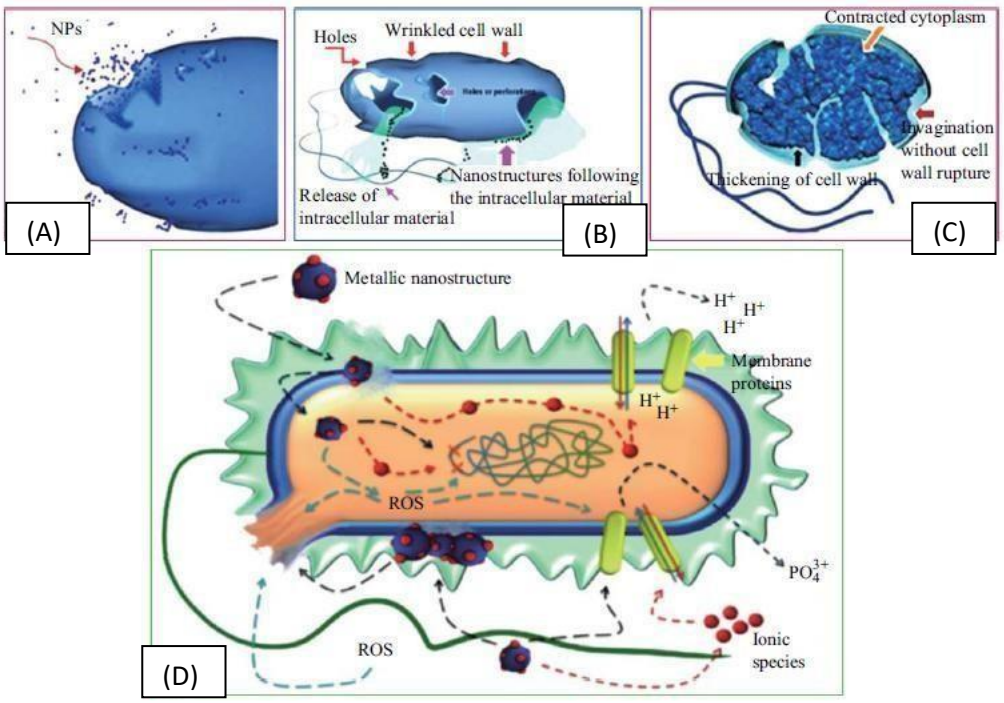

Figure 5.1: **(A)** NPs uptake through penetration into the cell and translocation. **(B)** Collapsed cell. **(C)** Variations in bacterial envelope composition and cytoplasm extrusion. **(D)** Possible toxicity mechanisms: metal ion internalization into cells, intracellular depletion, disruption of DNA replication, extrusion of metallic ions, ROS production, NP agglomeration and dissolution in the bacterial plasma membrane (Adopted from Dı´az-Visurraga et al., 2011).

5.5 Limitation and Future Recommendations

The growth curve profiling carried out in this research does not investigate the Zn^{2+} ion release which may be the main reason behind its toxicity (Kahru et al., 2008). The amount of toxic Zn^{2+} ion release should be quantified along with the growth inhibition assays to examine the ZnO NP effects on the bacterial growth curve and quantify the toxic Zn^{2+} ion release. We also did not analyse the cellular accumulation of zinc in the bacterial cell suspension. The ZnO NP content in the bacterial cells should be quantified to examine the relationship between the zinc accumulation in bacterial cells and cell viability. The toxicity mechanisms of ZnO NPs were not illustrated in this study. Future work should

include oxidative stress assessments such as lactate dehydrogenase leakage assay to assess the toxicity mechanism of ZnO NPs against the test organism. Lastly, high ZnO NP concentrations were proposed to be associated with a certain degree of skin epithelial cell toxicities (Hong et al., 2013; Moghaddam, 2017). We did not assess the effect of the ZnO NPs on the living organism. Therefore, animal testing should be conducted on ZnO NPs to determine their biocompatibility and applicability to human skin cells.

CHAPTER 6

CONCLUSION

The tested ZnO NP concentrations have statistically significant dose-dependent bacteriostatic but not bactericidal effects on *K. pneumoniae* with an MIC of 2560 μg/mL. Using the microbroth dilution method, the average percentage of growth inhibition reported on *K. pneumoniae* was 5, 13, 17, 23, 29, 36, 46, 65, 83, and 87% for 5, 10, 20, 40, 80, 160, 320, 640, 1280, and 2560 μg/ mL of ZnO NPs, respectively. ZnO NPs interacted with *K. pneumoniae* surface amine, hydroxyl, carbonyl, phosphate, and aliphatic groups of polysaccharides, proteins, glycogen, and phospholipids. Adsorption of ZnO NPs on cell membrane caused bacterial cells to aggregate, shrink, and distort. Besides, bacteria experienced damage, rupture, and roughening of cell surface after ZnO exposure. Overall, all the objectives proposed for the present study have been tested successfully. Besides, the results obtained in our study confirm the antibacterial activity of ZnO NPs against *K. pneumoniae.*

REFERENCES

Ademiluyi, A. and Oboh, G., 2013. Aqueous Extracts of Roselle (Hibiscus sabdariffa Linn.) Varieties Inhibit α-Amylase and α-Glucosidase Activities In Vitro. *Journal of Medicinal Food*, 16(1), pp.88-93.

Afreen, U., Bano, S., Tunio, S., Sharif, M. and Mirjat, A., 2020. Evaluation of Antibacterial Activity of Zinc Oxide Nanoparticles and Acrylamide Composite Against Multidrug-Resistant Pathogenic Bacteria. *Pakistan Journal of Analytical & Environmental Chemistry*, 21(1), pp.125-131.

Aguilar, C. et al., 2015. Organic-Inorganic Hybrid Nanoparticles for Bacterial Inhibition: Synthesis and Characterization of Doped and Undoped ONPs with Ag/Au NPs. *Molecules*, 20(4), pp.6002-6021.

Ahmadi, A., Ahmadi, P. and Ehsani, A., 2020. Development of an active packaging system containing zinc oxide nanoparticles for the extension of chicken fillet shelf life. *Food Science & Nutrition*, 8(10), pp.5461-5473.

Albertí, S. et al., 1996. Analysis of complement C3 deposition and degradation on Klebsiella pneumoniae. *Infection and Immunity*, 64(11), pp.4726-4732.

Albertí, S. et al., 1993. C1q binding and activation of the complement classical pathway by Klebsiella pneumoniae outer membrane proteins. *Infection and Immunity*, 61(3), pp.852-860.

Alias, S.S., Ismail, A.B. & Mohamad, A.A., 2010. Effect of pH on ZnO nanoparticle properties synthesized by Sol–gel centrifugation. *Journal of Alloys and Compounds*, 499(2), pp.231–237.

Al-Saiym, R., Al-Kamali, H. and Al-Magboul, A., 2015. Synergistic Antibacterial Interaction between Trachyspermum ammi, Senna alexandrina Mill and Vachellia nilotica spp. Nilotica Extract and Antibiotics. *Pakistan Journal of Biological Sciences*, 18(3), pp.115-121.

Al-Shabib, N. et al., 2016. Biogenic synthesis of Zinc oxide nanostructures from Nigella sativa seed: Prospective role as food packaging material inhibiting broad-spectrum quorum sensing and biofilm. *Scientific Reports*, 6(1).

Anbumani, D. et al., 2022. Green synthesis and antimicrobial efficacy of titanium dioxide nanoparticles using Luffa acutangula leaf extract. *Journal of King Saud University - Science*, 34(3), p.101896.

Ansari, M., Khan, H., Khan, A., Sultan, A. and Azam, A., 2011. Synthesis and characterization of the antibacterial potential of ZnO nanoparticles against extended-spectrum β-lactamases-producing *Escherichia coli* and *Klebsiella pneumoniae* isolated from a tertiary care hospital of North India. *Applied Microbiology and Biotechnology*, 94(2), pp.467-477.

Arakha, M. et al., 2015. Antimicrobial activity of iron oxide nanoparticle upon modulation of nanoparticle-bacteria interface. *Scientific Reports*, 5(1).

Arshad, M., Farrukh, M.A., Imtiaz, A. and Noor, N., 2015. Solvent assisted synthesis of tin-zinc oxide nanoparticles: Structural characterization and antimicrobial activity. *Asian Journal of Chemistry*, 27, pp. 371-374.

Azam, A. et al., 2012. Antimicrobial activity of metal oxide nanoparticles against Gram-positive and Gram-negative bacteria: a comparative study. *International Journal of Nanomedicine*, p.6003.

Azizi, S., Ahmad, M., Namvar, F. and Mohamad, R., 2014. Green biosynthesis and characterization of zinc oxide nanoparticles using brown marine macroalga Sargassum muticum aqueous extract. *Materials Letters*, 116, pp.275-277.

Bachman, M. et al., 2011. *Klebsiella pneumoniae* Yersiniabactin Promotes Respiratory Tract Infection through Evasion of Lipocalin 2. *Infection and Immunity*, 79(8), pp.3309-3316.

Bala, N. et al., 2015. Green synthesis of zinc oxide nanoparticles using Hibiscus subdariffa leaf extract: effect of temperature on synthesis, anti-bacterial activity and anti-diabetic activity. *RSC Advances*, 5(7), pp.4993-5003.

Banerjee, A. et al., 2021. Green synthesis of silver nanoparticles using exopolysaccharides produced by *bacillus anthracis* pfab2 and its biocidal property. *Journal of Polymers and the Environment*, 3, p.02051.

Bazant, P. et al., 2014. Wood flour modified by hierarchical Ag/ZnO as potential filler for wood–plastic composites with enhanced surface antibacterial performance. *Industrial Crops and Products*, 62, pp.179-187.

Behera, D., 2010. *Textbook of pulmonary medicine, volume 1,* 2 nd ed. New Delhi: JP Medical Ltd.

Bhat, R., 2013. Potential use of Fourier transform infrared spectroscopy for identification of molds capable of producing mycotoxins. *International Journal of Food Properties*, 16(8), pp.1819–1829.

Brock, J., Williams, P., Licéaga, J. and Wooldridge, K., 1991. Relative availability of transferrin-bound iron and cell-derived iron to aerobactin-producing and enterochelin-producing strains of *Escherichia coli* and to other microorganisms. *Infection and Immunity*, 59(9), pp.3185-3190.

Burattini, E. et al., 2008. A FTIR microspectroscopy study of autolysis in cells of the wine yeast *Saccharomyces cerevisiae*. *Vibrational Spectroscopy*, *47*(2), pp.139-147.

Buzea, C., Pacheco, I. and Robbie, K., 2007. Nanomaterials and nanoparticles: Sources and toxicity. Biointerphases, 2(4), pp.MR17-MR71.

Chetcuti Zammit, S., Azzopardi, N. and Sant, J., 2014. Mortality risk score for *Klebsiella pneumoniae* bacteraemia. *European Journal of Internal Medicine*, 25(6), pp.571-576.

Chithra, M., Sathya, M. and Pushpanathan, K., 2015. Effect of pH on Crystal Size and Photoluminescence Property of ZnO Nanoparticles Prepared by Chemical Precipitation Method. *Acta Metallurgica Sinica (English Letters)*, 28(3), pp.394-404.

Choudhary, N., Sharma, S., Dwivedi, J., Jha, A. and Goyal, S., 2011. Anti-diabetic potential of chloroform extract of flowers of Calotropis gigantea: An in vitro and in vivo study. *International Journal of Green Pharmacy*, 5(4), pp.296-301.

Cioffi, N. and Rai, M., 2012. Nano-antimicrobials: progress and prospects [e-book]. London, New York: Springer-Verlag Berlin Heidelberg. Available at: Google books https://books.google.com.my [Accessed: 16 March 2022].

Clements, A. et al., 2008. The Major Surface-Associated Saccharides of *Klebsiella pneumoniae* Contribute to Host Cell Association. *PLoS ONE*, 3(11), p.e3817.

Clements, A. et al., 2007. Secondary Acylation of *Klebsiella pneumoniae* Lipopolysaccharide Contributes to Sensitivity to Antibacterial Peptides. *Journal of Biological Chemistry*, 282(21), pp.15569-15577.

Colodner, R., Raz, R., Chazan, B. and Sakran, W., 2004. Susceptibility pattern of ESBL-producing bacteria isolated from inpatients to five antimicrobial drugs in a community hospital in northern Israel. *International Journal of Antimicrobial Agents*, 24(4), pp.409-410.

Condello, M. et al., 2016. ZnO nanoparticle tracking from uptake to genotoxic damage in human colon carcinoma cells. *Toxicology in Vitro*, 35, pp.169-179.

Cortés, G. et al., 2002. Molecular Analysis of the Contribution of the Capsular Polysaccharide and the Lipopolysaccharide O Side Chain to the Virulence of *Klebsiella pneumoniae* in a Murine Model of Pneumonia. *Infection and Immunity*, 70(5), pp.2583-2590.

Coutinho, H., Lima, E. and Siqueira-Júnior, J., 2010. Additive effects of Hyptis martiusii Benth with aminoglycosides against *Escherichia coli*. *Indian Journal of Medical Research*, 131, pp.106-108.

Dadi, R., Azouani, R., Traore, M., Mielcarek, C. and Kanaev, A., 2019. Antibacterial activity of ZnO and CuO nanoparticles against gram positive and gram negative strains. *Materials Science and Engineering: C*, 104, pp. 1-9.

Dalai, S., Pakrashi, S., Kumar, R., Chandrasekaran, N. and Mukherjee, A., 2012. A comparative cytotoxicity study of TiO2 nanoparticles under light and dark conditions at low exposure concentrations. *Toxicology Research*, 1(2), p.116.

Desselberger, U., 2000. Emerging and Re-emerging Infectious Diseases. Journal of Infection, 40(1), pp.3-15.

Dhanasegaran, K. et al., 2021. Antibacterial properties of zinc oxide nanoparticles on *Pseudomonas aeruginosa* (ATCC 27853). *Scientia Iranica F*, 28(6).

Dhas, S., Shiny, P., Khan, S., Mukherjee, A. and Chandrasekaran, N., 2013. Toxic behavior of silver and zinc oxide nanoparticles on environmental microorganisms. *Journal of Basic Microbiology*, 54(9), pp.916-927.

Díaz, M., Hernández, J., Martínez-Martínez, L., Rodríguez-Baño, J. and Pascual, Á., 2009. *Escherichia coli* y *Klebsiella pneumoniae* productoras de betalactamasas de espectro extendido en hospitales españoles: segundo estudio multicéntrico (proyecto GEIH-BLEE 2006). *Enfermedades Infecciosas y Microbiología Clínica*, 27(9), pp.503-510.

Dimapilis, E.A. et al., 2018. Zinc oxide nanoparticles for water disinfection. *Sustainable Environment Research*, 28(2), pp.47–56.

Dizaj, S.M., Lotfipour, F., Barzegar-Jalali, M., Zarrintan, M, H. and Adibkia, K., 2014. Antimicrobial activity of the metals and metal oxide nanoparticles. *Materials Science and Engineering C*, 44, pp. 278-284.

Djearamane, S., Lim, Y.M., Wong, L.S. and Lee, P.F., 2018. Cytotoxic effects of zinc oxide nanoparticles on cyanobacterium Spirulina (Arthrospira) platensis. *PeerJ*, *6*, p.e4682.

Djearamane, S., Wong, L., Lim, Y. and Lee, P., 2019. Short-Term Cytotoxicity of Zinc Oxide Nanoparticles on Chlorella vulgaris. *Sains Malaysiana*, 48(1), pp.69-73.

Donnenberg, M., 2015. Enterobacteriaceae. *Mandell, Douglas, and Bennett's Principles and Practice of Infectious Diseases*, 2, pp.2503-2517.e5.

Edmunds, P., 1954. Further Klebsiella Capsule Types. *Journal of Infectious Diseases*, 94(1), pp.65-71.

Edwards, P. and Fife, M., 1952. Capsule Types of Klebsiella. Journal of Infectious Diseases, 91(1), pp.92-104.

El Fertas-Aissani, R., Messai, Y., Alouache, S. and Bakour, R., 2013. Virulence profiles and antibiotic susceptibility patterns of *Klebsiella pneumoniae* strains isolated from different clinical specimens. *Pathologie Biologie*, 61(5), pp.209-216.

Esmailzadeh, H. et al., 2016. Effect of nanocomposite packaging containing ZnO on growth of *bacillus subtilis* and *Enterobacter aerogenes*. *Materials Science and Engineering: C*, 58, pp.1058–1063.

Evrard, B. et al., 2010. Roles of Capsule and Lipopolysaccharide O Antigen in Interactions of Human Monocyte-Derived Dendritic Cells and *Klebsiella pneumoniae*. *Infection and Immunity*, 78(1), pp.210-219.

Fang, C., Chuang, Y., Shun, C., Chang, S. and Wang, J., 2004. A Novel Virulence Gene in Klebsiella pneumoniae Strains Causing Primary Liver Abscess and Septic Metastatic Complications. *Journal of Experimental Medicine*, 199(5), pp.697-705.

Fang, C. et al., 2007. *Klebsiella pneumoniae* Genotype K1: An Emerging Pathogen That Causes Septic Ocular or Central Nervous System Complications from Pyogenic Liver Abscess. *Clinical Infectious Diseases*, 45(3), pp.284-293.

Favre-Bonté, S., Licht, T., Forestier, C. and Krogfelt, K., 1999. *Klebsiella pneumoniae* Capsule Expression Is Necessary for Colonization of Large Intestines of Streptomycin-Treated Mice. *Infection and Immunity*, 67(11), pp.6152-6156.

FDA (Food and Drug Administration), 2022. *eCFR :: 21 CFR 582.5991 -- Zinc oxide.*. [online] Ecfr.gov. Available at: <https://www.ecfr.gov/current/title-21/chapter-I/subchapter-E/part-582/subpart-F/section-582.5991> [Accessed 20 January 2022].

Feng, Y. et al., 2014. An in situ gelatin-assisted hydrothermal synthesis of ZnO–reduced graphene oxide composites with enhanced photocatalytic performance under Ultraviolet and visible light. *RSC Advances*, 4(16), p.7933.

Fernando, S., Gunasekara, T. and Holton, J., 2018. Antimicrobial Nanoparticles: applications and mechanisms of action. Sri Lankan Journal of Infectious Diseases, 8(1), p.2.

Fiedot, M. et al., 2017. The Relationship between the Mechanism of Zinc Oxide Crystallization and Its Antimicrobial Properties for the Surface Modification of Surgical Meshes. *Materials*, 10(4), p.353.

Fischbach, M., Lin, H., Liu, D. and Walsh, C., 2005. In vitro characterization of IroB, a pathogen-associated C-glycosyltransferase. *Proceedings of the National Academy of Sciences*, 102(3), pp.571-576.

Fischbach, M. et al., 2006. The pathogen-associated iroA gene cluster mediates bacterial evasion of lipocalin 2. *Proceedings of the National Academy of Sciences*, 103(44), pp.16502-16507.

Friedlaender, C., 1882. Ueber die Schizomyceten bei der acuten fibrösen Pneumonie. *Archiv für Pathologische Anatomie und Physiologie und für Klinische Medicin*, 87(2), pp.319-324.

Fuzi, M., Rodriguez Baño, J. and Toth, A., 2020. Global Evolution of Pathogenic Bacteria with Extensive Use of Fluoroquinolone Agents. *Frontiers in Microbiology*, 11.

Garcia, C., Shin, G. and Kim, J., 2018. Metal oxide-based nanocomposites in food packaging: Applications, migration, and regulations. *Trends in Food Science & Technology*, 82, pp.21-31.

Garip, S., Gozen, A.C. and Severcan, F., 2009. Use of Fourier transform infrared spectroscopy for rapid comparative analysis of *Bacillus* and *Micrococcus* isolates. *Food Chemistry*, 113, pp. 1301-1307.

Ghasemi, F. and Jalal, R., 2016. Antimicrobial Action of Zinc Oxide Nanoparticles in Combination with Ciprofloxacin and Ceftazidime against Multidrug-resistant *Acinetobacter baumannii*. *Journal of Global Antimicrobial Resistance*, 6, pp.118-122.

Gorgulu, S.T., Dogan, M. and Severcan, F., 2007. The characterization and differentiation of higher plants by Fourier transform infrared spectroscopy. *Applied Spectroscopy*, 61(3), pp. 300-308.

Gupta, M. et al., 2018. Effective antimicrobial activity of green ZnO nano particles of Catharanthus roseus. Frontiers in Microbiology, 9.

Gupta, S., Sharma, S. and Singh, S., 2014. Hexavalent Chromium Toxicity to Cyanobacterium Spirulina Platensis. *International Research Journal of Pharmacy*, 5(12), pp.910-914.

Hameed, A.S. et al., 2016. In vitro antibacterial activity of ZnO and Nd doped ZnO nanoparticles against ESBL producing *Escherichia coli* and *Klebsiella pneumoniae*. *Scientific Reports*, 6(1).

Hansen, D. et al., 1999. *Klebsiella pneumoniae* Lipopolysaccharide O Typing: Revision of Prototype Strains and O-Group Distribution among Clinical Isolates from Different Sources and Countries. *Journal of Clinical Microbiology*, 37(1), pp.56-62.

Happy Agarwal, Soumya Menon, Venkat Kumar, S. and Rajeshkumar, S., 2018. Mechanistic study on antibacterial action of zinc oxide nanoparticles synthesized using green route. *Chemico-Biological Interactions*, 286, pp.60-70.

Hong, Z. et al., 2013. The effect of extracellular polymeric substances on the adhesion of bacteria to clay minerals and goethite. Chemical Geology, 360-361, pp.118-125.

Hu, X., Jia, X., Zhi, C., Jin, Z. and Miao, M., 2019. Improving the properties of starch-based antimicrobial composite films using ZnO-chitosan nanoparticles. *Carbohydrate Polymers*, 210, pp.204-209.

Huang, Z. et al., 2003. Near-infrared Raman spectroscopy for optical diagnosis of lung cancer. International Journal of Cancer, 107(6), pp.1047-1052.

Hudzicki, J., 2009. *Kirby-Bauer Disk Diffusion Susceptibility Test Protocol*. [Online]. American Society for Microbiology. Available at: <https://asm.org/Protocols/Kirby-Bauer-Disk-Diffusion-Susceptibility-Test-Pro> [Accessed 9 October 2022].

Ifeanyichukwu, U.L., Fayemi, O.E. and Ateba, C.N., 2020. Green synthesis of zinc oxide nanoparticles from pomegranate (Punica granatum) extracts and characterization of their antibacterial activity. Molecules, 25(19), pp.1-22.

Ilves, M. et al., 2014. Topically applied ZnO nanoparticles suppress allergen induced skin inflammation but induce vigorous IgE production in the atopic dermatitis mouse model. *Particle and Fibre Toxicology*, 11(1).

Imade, E., Ajiboye, T., Fadiji, A., Onwudiwe, D. and Babalola, O., 2022. Green synthesis of zinc oxide nanoparticles using plantain peel extracts and the evaluation of their antibacterial activity. *Scientific African*, 16, p.e01152.

James, M. and Cohen, J., 1980. The measurement of residual stresses by X-ray diffraction techniques. *Treatise on Materials Science & Technology*, pp.1–62.

Janda, J. and Abbott, S., 2006. *The Enterobacteria*. 2nd ed. Washington, D.C.: ASM Press, pp.115-129.

Jones, N., Ray, B., Ranjit, K. and Manna, A., 2008. Antibacterial activity of ZnO nanoparticle suspensions on a broad spectrum of microorganisms. FEMS Microbiology Letters, 279(1), pp.71-76.

Kahru, A., Dubourguier, H., Blinova, I., Ivask, A. and Kasemets, K., 2008. Biotests and Biosensors for Ecotoxicology of Metal Oxide Nanoparticles: A Minireview. Sensors, 8(8), pp.5153-5170.

Kasi, G., Viswanathan, K. and Seo, J., 2019. Effect of annealing temperature on the morphology and antibacterial activity of Mg-doped zinc oxide nanorods. *Ceramics International*, 45(3), pp.3230-3238.

Khan, S. et al., 2020. Inhibition of multi-drug resistant *Klebsiella pneumoniae*: Nanoparticles induced photoinactivation in presence of efflux pump inhibitor. *European Journal of Pharmaceutics and Biopharmaceutics*, 157, pp.165-174.

Ko, W. et al., 2002. Community-Acquired *Klebsiella pneumoniae* Bacteremia: Global Differences in Clinical Patterns. *Emerging Infectious Diseases*, 8(2), pp.160-166.

Koczura, R. and Kaznowski, A., 2003. Occurrence of the Yersinia high-pathogenicity island and iron uptake systems in clinical isolates of Klebsiella pneumoniae. Microbial Pathogenesis, 35(5), pp.197-202.

Korvick, J., Hackett, A., Yu, V. and Muder, R., 1991. Klebsiella Pneumonia in the Modern Era. Southern Medical Journal, 84(2), pp.200-204.

Krishnamoorthy, V. et al., 2012. Epinephrine Induces Rapid Deterioration in Pulmonary Oxygen Exchange in Intact, Anesthetized Rats. Anesthesiology, 117(4), pp.745-754.

Kumari, J. et al., 2014. Cytotoxicity of TiO2 nanoparticles towards freshwater sediment microorganisms at low exposure concentrations. *Environmental Research*, 135, pp.333-345.

Lawlor, M., O'Connor, C. and Miller, V., 2007. Yersiniabactin Is a Virulence Factor for *Klebsiella pneumoniae* during Pulmonary Infection. *Infection and Immunity*, 75(3), pp.1463-1472.

Lee, K. et al., 2017. *MALAYSIAN ACTION PLAN ON ANTIMICROBIAL RESISTANCE (MyAP-AMR) 2017-2021*. Malaysia: Ministry of Health, Malaysia and Ministry of Agriculture & Agro-Based Industry Malaysia, p.11.

Li, B., Zhao, Y., Liu, C., Chen, Z. and Zhou, D., 2014. Molecular pathogenesis of Klebsiella pneumoniae. *Future Microbiology*, 9(9), pp.1071-1081.

Li, M., Zhu, L. and Lin, D., 2011. Toxicity of ZnO Nanoparticles to *Escherichia coli*: Mechanism and the Influence of Medium Components. *Environmental Science & Technology*, 45(5), pp.1977-1983.

Li, W.R. et al., 2010. Antibacterial activity and mechanism of silver nanoparticles on *Escherichia coli*. *Applied microbiology and biotechnology*, *85*(4), pp.1115-1122.

Liang, S. X. T., Wong, L. S., Lim, Y. M., Lee, P. F. and Djearamane, S., 2020. Effects of zinc oxide nanoparticles on *Streptococcus pyogenes*. *South African Journal of Chemical Engineering*, *34*, pp.63-71.

Llobet, E. et al., 2015. Deciphering tissue-induced Klebsiella pneumoniae lipid A structure. Proceedings of the National Academy of Sciences, 112(46), pp.E6369-E6378.

Magill, S. et al., 2014. Multistate Point-Prevalence Survey of Health Care–Associated Infections. New England Journal of Medicine, 370(13), pp.1198-1208.

Maity, J.P. et al., 2013. Identification and discrimination of bacteria using Fourier transform infrared spectroscopy. Spectrochimica Acta Part A: Molecular and Biomolecular Spectroscopy, 116, pp.478–484.

Marchaim, D. et al., 2011. Outbreak of Colistin-Resistant, Carbapenem-Resistant *Klebsiella pneumoniae* in Metropolitan Detroit, Michigan. *Antimicrobial Agents and Chemotherapy*, 55(2), pp.593-599.

Meatherall, B., Gregson, D., Ross, T., Pitout, J. and Laupland, K., 2009. Incidence, Risk Factors, and Outcomes of *Klebsiella pneumoniae* Bacteremia. *The American Journal of Medicine*, 122(9), pp.866-873.

Melin, A.-M., Perromat, A. & Déléris, G., 2000. Pharmacologic application of Fourier transform IR spectroscopy:in vivo toxicity of carbon tetrachloride on rat liver. *Biopolymers*, 57(3), pp.160–168.

Merino, S., Camprubí, S., Albertí, S., Benedí, V. and Tomás, J., 1992. Mechanisms of *Klebsiella pneumoniae* resistance to complement-mediated killing. *Infection and Immunity*, 60(6), pp.2529-2535.

Merle, N., Noe, R., Halbwachs-Mecarelli, L., Fremeaux-Bacchi, V. and Roumenina, L., 2015. Complement System Part II: Role in Immunity. *Frontiers in Immunology*, 6.

Mezzatesta, M. et al., 2011. Outbreak of KPC-3-producing, and colistin-resistant, *Klebsiella pneumoniae* infections in two Sicilian hospitals. *Clinical Microbiology and Infection*, 17(9), pp.1444-1447.

Mirzaei, H. and Darroudi, M., 2017. Zinc oxide nanoparticles: Biological synthesis and biomedical applications. *Ceramics International*, 43(1), pp.907-914.

Mishra, P., Mishra, H., Ekielski, A., Talegaonkar, S. and Vaidya, B., 2017. Zinc oxide nanoparticles: a promising nanomaterial for biomedical applications. Drug Discovery Today, 22(12), pp.1825-1834.

Mohd Yusof, H., Mohamad, R., Zaidan, U. and Abdul Rahman, N., 2019. Microbial synthesis of zinc oxide nanoparticles and their potential application as an antimicrobial agent and a feed supplement in animal industry: a review. Journal of Animal Science and Biotechnology, 10(1), pp.1-22.

Mohd Yusof, H., Abdul Rahman, N., Mohamad, R., Hasanah Zaidan, U. and Samsudin, A., 2021. Antibacterial Potential of Biosynthesized Zinc Oxide Nanoparticles against Poultry-Associated Foodborne Pathogens: An In Vitro Study. *Animals*, 11(7), p.2093.

Montminy, S. et al., 2006. Virulence factors of Yersinia pestis are overcome by a strong lipopolysaccharide response. *Nature Immunology*, 7(10), pp.1066-1073.

Murphy, C. and Clegg, S., 2012. *Klebsiella pneumoniae* and type 3 fimbriae: nosocomial infection, regulation and biofilm formation. *Future Microbiology*, 7(8), pp.991-1002.

Nandiyanto, A., Oktiani, R. and Ragadhita, R., 2019. How to Read and Interpret FTIR Spectroscope of Organic Material. *Indonesian Journal of Science and Technology*, 4(1), p.97.

Narayanan, P., Wilson, W., Abraham, A. and Sevanan, M., 2012. Synthesis, Characterization, and Antimicrobial Activity of Zinc Oxide Nanoparticles Against Human Pathogens. *BioNanoScience*, 2(4), pp.329-335.

Nassif, X., Fournier, J., Arondel, J. and Sansonetti, P., 1989. Mucoid phenotype of *Klebsiella pneumoniae* is a plasmid-encoded virulence factor. *Infection and Immunity*, 57(2), pp.546-552.

Nassif, X. and Sansonetti, P., 1986. Correlation of the virulence *of Klebsiella pneumoniae* K1 and K2 with the presence of a plasmid encoding aerobactin. *Infection and Immunity*, 54(3), pp.603-608.

Naumann, D., 2001. FT-Infrared and FT-Raman spectroscopy in biomedical research. Applied Spectroscopy Reviews, 36(2-3), pp. 239-298.

Nava, O. et al., 2017. Fruit peel extract mediated green synthesis of zinc oxide nanoparticles. Journal of Molecular Structure, 1147, pp.1-6.

National Nanotechnology Initiative, 2011, What Is Nanotechnology?. [Online]. Available at: <https://www.nano.gov/nanotech-101/what/definition> [Accessed 1 January 2022].

Ngo, T., Dang, T., Tran, T. and Rachtanapun, P., 2018. Effects of Zinc Oxide Nanoparticles on the Properties of Pectin/Alginate Edible Films. *International Journal of Polymer Science*, 2018, pp.1-9.

Ngo Thi, N. and Naumann, D., 2006. Investigating the heterogeneity of cell growth in microbial colonies by FTIR microspectroscopy. *Analytical and Bioanalytical Chemistry*, 387(5), pp.1769-1777.

Ngoi, S. et al., 2021. In Vitro Efficacy of Flomoxef against Extended-Spectrum Beta-Lactamase-Producing *Escherichia coli* and *Klebsiella pneumoniae* Associated with Urinary Tract Infections in Malaysia. *Antibiotics*, 10(2), p.181.

Nie, L. et al, 2020. Silver-doped biphasic calcium phosphate/alginate microclusters with antibacterial property and controlled doxorubicin delivery. *Journal of Applied Polymer Science*, 138(19), p.50433.

Nordmann, P., Cuzon, G. and Naas, T., 2009. The real threat of *Klebsiella pneumoniae* carbapenemase-producing bacteria. *The Lancet Infectious Diseases*, 9(4), pp.228-236.

Obeizi, Z. et al., 2020. Biosynthesis of Zinc oxide nanoparticles from essential oil of Eucalyptus globulus with antimicrobial and anti-biofilm activities. *Materials Today Communications*, 25, p.101553.

Ojeda, J.J., Romero-Gonzalez, M.E., Pouran, H.M. and Banwart, S.A., 2008. *In situ* monitoring of the biofilm formation of *Pseudomonas putida* on hematite using flow-cell ATR-FTIR spectroscopy to investigate the formation of inner-sphere bonds between the bacteria and the mineral. *Mineralogical Magazine*, 72(1), pp.101-106.

O'Neill, J., 2014. *Review on Antimicrobial Resistance Antimicrobial Resistance: Tackling a crisis for the health and wealth of nations*. Review on Antimicrobial Resistance. [Online]. Available at: <https://amr-review.org/sites/default/files/AMR%20Review%20Paper%20-%20Tackling%20a%20crisis%20for%20the%20health%20and%20wealth%20of%20nations_1.pdf> [Accessed 7 January 2022].

Orskov, I. and Fife-Asbury, M., 1977. New Klebsiella Capsular Antigen, K82, and the Deletion of Five of Those Previously Assigned. International Journal of Systematic Bacteriology, 27(4), pp.386-387.

Osuntokun, J., Onwudiwe, D.C. and Ebenso, E.E., 2019. Green synthesis of ZnO nanoparticles using aqueous Brassica oleracea L. var. italica and the photocatalytic activity. Green Chemistry Letters and Reviews, 12(4), pp.444-457.

Paczosa, M. and Mecsas, J., 2016. *Klebsiella pneumoniae*: Going on the Offense with a Strong Defense. *Microbiology and Molecular Biology Reviews*, 80(3), pp.629-661.

Paisoonsin, S., Pornsunthorntawee, O. and Rujiravanit, R., 2013. Preparation and characterization of ZnO-deposited DBD plasma-treated PP packaging film with antibacterial activities. *Applied Surface Science*, 273, pp.824-835.

Pan, Y., Lin, T., Hsu, C. and Wang, J., 2011. Use of a Dictyostelium Model for Isolation of Genetic Loci Associated with Phagocytosis and Virulence in *Klebsiella pneumoniae*. *Infection and Immunity*, 79(3), pp.997-1006.

Pandey, K. and Rizvi, S., 2009. Plant Polyphenols as Dietary Antioxidants in Human Health and Disease. *Oxidative Medicine and Cellular Longevity*, 2(5), pp.270-278.

Patra, J., Baek, K. and Perera, C., 2017. Antibacterial Activity and Synergistic Antibacterial Potential of Biosynthesized Silver Nanoparticles against Foodborne Pathogenic Bacteria along with its Anticandidal and Antioxidant Effects. *Frontiers in Microbiology*, 08.

Pelgrift, R. and Friedman, A., 2013. Nanotechnology as a therapeutic tool to combat microbial resistance. *Advanced Drug Delivery Reviews*, 65(13-14), pp.1803-1815.

Peng, K. et al., 2018. Development of direct contact-killing non-leaching antimicrobial polyurethanes through Click Chemistry. Journal of Coatings Technology and Research, 15(6), pp.1239–1250.

Peng, X., Palma, S., Fisher, N. and Wong, S., 2011. Effect of morphology of ZnO nanostructures on their toxicity to marine algae. Aquatic Toxicology, 102(3-4), pp.186-196.

Perry, R., Balbo, P., Jones, H., Fetherston, J. and DeMoll, E., 1999. Yersiniabactin from *Yersinia pestis*: biochemical characterization of the siderophore and its role in iron transport and regulation. *Microbiology*, 145(5), pp.1181-1190.

Podschun, R., Pietsch, S., Höller, C. and Ullmann, U., 2001. Incidence of Klebsiella Species in Surface Waters and Their Expression of Virulence Factors. *Applied and Environmental Microbiology*, 67(7), pp.3325-3327.

Podschun, R. and Ullmann, U., 1998. Klebsiella spp. as Nosocomial Pathogens: Epidemiology, Taxonomy, Typing Methods, and Pathogenicity Factors. *Clinical Microbiology Reviews*, 11(4), pp.589-603.

Qu, F. and Morais, P., 1999. Energy levels in metal oxide semiconductor quantum dots in water-based colloids. *The Journal of Chemical Physics*, 111(18), pp.8588-8594.3

Qureshi, S., 2019, *Klebsiella Infections: Background, Pathophysiology, Epidemiology of Klebsiellae*. [Online]. Available at: <https://emedicine.medscape.com/article/219907-overview> [Accessed 15 January 2022].

Raghupathi, K. R., Koodali, R. T. and Manna, A. C., 2011. Size-dependent bacterial growth inhibition and mechanism of antibacterial activity of zinc oxide nanoparticles. *Langmuir*, *27*(7), pp.4020-4028.

Rajakumar, G. et al., 2012. Eclipta prostrata leaf aqueous extract mediated synthesis of titanium dioxide nanoparticles. *Materials Letters*, 68, pp.115-117.

Ranjbar, R., Izadi, M., Hafshejani, T. and Khamesipour, F., 2016a. Molecular detection and antimicrobial resistance of *Klebsiella pneumoniae* from house flies (Musca domestica) in kitchens, farms, hospitals and slaughterhouses. *Journal of Infection and Public Health*, 9(4), pp.499-505.

Ranjbar, R., Memariani, H., Sorouri, R. and Memariani, M., 2016b. Distribution of virulence genes and genotyping of CTX-M-15-producing Klebsiella pneumoniae isolated from patients with community-acquired urinary tract infection (CA-UTI). Microbial Pathogenesis, 100, pp.244-249.

Ranjbar, R., Kelishadrokhi, A.F. & Chehelgerdi, M., 2019. Molecular characterization, serotypes and phenotypic and genotypic evaluation of antibiotic resistance of the *klebsiella pneumoniae* strains isolated from different types of hospital-acquired infections. *Infection and Drug Resistance*, 12(1), pp.603–611.

Rasha, E. et al., 2021a. Effects of Zinc Oxide Nanoparticles Synthesized Using *Aspergillus niger* on Carbapenem-Resistant *Klebsiella pneumonia* In Vitro and In Vivo. *Frontiers in Cellular and Infection Microbiology*, 11.

Rasha, E. et al., 2021b. Biosynthesis of Zinc Oxide Nanoparticles from Acacia nilotica (L.) Extract to Overcome Carbapenem-*Resistant Klebsiella Pneumoniae*. *Molecules*, 26(7), p.1919.

Rasmussen, J., Martinez, E., Louka, P. and Wingett, D., 2010. Zinc oxide nanoparticles for selective destruction of tumor cells and potential for drug delivery applications. *Expert Opinion on Drug Delivery*, 7(9), pp.1063-1077.

Reddy, L.S. et al., 2014. Antimicrobial activity of zinc oxide (zno) nanoparticle against *klebsiella pneumoniae*. *Pharmaceutical Biology*, 52(11), pp.1388–1397.

Regueiro, V. et al., 2010. Klebsiella pneumoniae subverts the activation of inflammatory responses in a NOD1-dependent manner. *Cellular Microbiology*, 13(1), pp.135-153.

Ríos, J. and Recio, M., 2005. Medicinal plants and antimicrobial activity. *Journal of Ethnopharmacology*, 100(1-2), pp.80-84.

Rock, C. et al., 2014. Frequency of Klebsiella pneumoniae Carbapenemase (KPC)–Producing and Non-KPC-Producing Klebsiella Species Contamination of Healthcare Workers and the Environment. *Infection Control & Hospital Epidemiology*, 35(4), pp.426-429.

Russo, T. et al., 2011. Hypervirulent K. Pneumoniae Secretes More and More Active Iron-Acquisition Molecules than "Classical" K. Pneumoniae Thereby Enhancing its Virulence. PLoS ONE, 6(10), p.e26734.

Russo, T. et al., 2014. Aerobactin Mediates Virulence and Accounts for Increased Siderophore Production under Iron-Limiting Conditions by Hypervirulent (Hypermucoviscous) *Klebsiella pneumoniae*. *Infection and Immunity*, 82(6), pp.2356-2367.

Russo, T., Olson, R., MacDonald, U., Beanan, J. and Davidson, B., 2015. Aerobactin, but Not Yersiniabactin, Salmochelin, or Enterobactin, Enables the Growth/Survival of Hypervirulent (Hypermucoviscous) *Klebsiella pneumoniae* Ex Vivo and In Vivo. *Infection and Immunity*, 83(8), pp.3325-3333.

Sahdev, P., Posaralla S., Kaushik, R.S. and Perumal, O., 2013. Calcium phosphate nanoparticles for transcutaneous vaccine delivery. *Journal of Biomedical Nanotechnology*, 9(1), pp. 132-141.

Sahly, H. et al., 2000. Capsule Impedes Adhesion to and Invasion of Epithelial Cells by *Klebsiella pneumoniae*. *Infection and Immunity*, 68(12), pp.6744-6749.

Sánchez-Sanhueza, G. et al., 2018. Synthesis of Copper Nanowires and Their Antimicrobial Activity on Strains Isolated Persistent Endodontic Infections. *Journal of Nanoscience and Nanotechnology*, 18(7), pp.4507-4514.

Sangeetha, G., Rajeshwari, S. and Venckatesh, R., 2011. Green synthesis of zinc oxide nanoparticles by aloe barbadensis miller leaf extract: Structure and optical properties. *Materials Research Bulletin*, 46(12), pp.2560-2566.

Saravanan, D., Lakshmi, I., Gobinath, M. and Kumar, B., 2011. Potential Antioxidant, Hypoglycemic and Hypolipidemic Effect of Leaves of Hibiscus platanifolius Linn. *Int. J. Pharm. Sci. Drug Res.*, 3(3), pp.236–240.

Sasidharan, A. et al., 2011. Rapid dissolution of ZnO nanocrystals in acidic cancer microenvironment leading to preferential apoptosis. *Nanoscale*, 3(9), pp.3657-3669.

Senthamarai, M.D. & Malaikozhundan, B., 2022. Synergistic action of zinc oxide nanoparticle using the unripe fruit extract of Aegle Marmelos (L.) - antibacterial, antibiofilm, radical scavenging and ecotoxicological effects. Materials Today Communications, 30, p.103228.

Shahvalizadeh, R. et al., 2021. Antimicrobial bio-nanocomposite films based on gelatin, tragacanth, and zinc oxide nanoparticles – Microstructural, mechanical, thermo-physical, and barrier properties. *Food Chemistry*, 354, p.129492.

Shankar, S. and Rhim, J. W., 2019. Effect of types of zinc oxide nanoparticles on structural, mechanical and antibacterial properties of poly (lactide)/poly (butylene adipate-co-terephthalate) composite films. *Food Packaging and Shelf Life*, 21, pp.1-7.

Shankar-Sinha, S. et al., 2004. The *Klebsiella pneumoniae* O Antigen Contributes to Bacteremia and Lethality during Murine Pneumonia. *Infection and Immunity*, 72(3), pp.1423-1430.

Sharma, D. and Chaudhary, A., 2020. One Pot Synthesis of Gentamicin Conjugated Gold Nanoparticles as an Efficient Antibacterial Agent. *Journal of Cluster Science*, 32(4), pp.995-1002.

Sharma, N. et al, 2019. Preparation and Evaluation of the ZnO NP–Ampicillin/Sulbactam Nanoantibiotic: Optimization of Formulation Variables Using RSM Coupled GA Method and Antibacterial Activities. *Biomolecules*, 9(12), p.764.

Shivaee, A., Kashani, S., Mohammadzadeh, R. and Ebrahimi, M., 2021. Effect of Zinc Oxide Nanoparticle on the Expression of mrkA and fimA in Drug-Resistant *Klebsiella pneumoniae*. *Journal of Medical Bacteriology*, 10(3, 4), pp.1-10.

Shon, A., Bajwa, R. and Russo, T., 2013. Hypervirulent (hypermucoviscous)*Klebsiella pneumoniae*. *Virulence*, 4(2), pp.107-118.

Siddiqi, K., ur Rahman, A., Tajuddin and Husen, A., 2018. Properties of Zinc Oxide Nanoparticles and Their Activity Against Microbes. *Nanoscale Research Letters*, 13(1).

Silvera Batista, C., Larson, R. and Kotov, N., 2015. Nonadditivity of nanoparticle interactions. Science, 350, pp.1242477 –1242477.

Simoons-Smit, A., Verweij-Van Vught, A. and Maclaren, D., 1986. The role of K antigens as virulence factors in Klebsiella. Journal of Medical Microbiology, 21(2), pp.133-137.

Singh, T., Das, J. and Sil, P., 2020. Zinc oxide nanoparticles: A comprehensive review on its synthesis, anticancer and drug delivery applications as well as health risks. *Advances in Colloid and Interface Science*, 286, p.102317.

Sirelkhatim, A. et al., 2015. Review on Zinc Oxide Nanoparticles: Antibacterial Activity and Toxicity Mechanism. *Nano-Micro Letters*, 7(3), pp.219-242.

Smith, K. and Kirby, J., 2018. The Inoculum Effect in the Era of Multidrug Resistance: Minor Differences in Inoculum Have Dramatic Effect on MIC Determination. *Antimicrobial Agents and Chemotherapy*, 62(8).

Sobhanifar, S. et al., 2015. Structure and mechanism of *staphylococcus aureus* tarm, the wall teichoic acid α-glycosyltransferase. *Proceedings of the National Academy of Sciences*, 112(6), pp.E576–E585.

Sogne, V., Meier, F., Klein, T. and Contado, C., 2017. Investigation of zinc oxide particles in cosmetic products by means of centrifugal and asymmetrical flow field-flow fractionation. *Journal of Chromatography A*, 1515, pp.196-208.

Spagnolo, A., Orlando, P., Panatto, D., Perdelli, F. and Cristina, M., 2014. An overview of carbapenem-resistant *Klebsiella pneumoniae*. *Reviews in Medical Microbiology*, 25(1), pp.7-14.

Srinivas, V., 2020. *Gram Staining|Bacterial Staining Technique*. [online] Youtube.com. Available at: <https://www.youtube.com/watch?v=--OvDvS-Pec&t=481s> [Accessed 12 January 2022].

Tang, S. et al., 2019. Ecofriendly and Biodegradable Soybean Protein Isolate Films Incorporated with ZnO Nanoparticles for Food Packaging. *ACS Applied Bio Materials*, 2(5), pp.2202-2207.

Tarkkanen, A. et al., 1992. Fimbriation, capsulation, and iron-scavenging systems of Klebsiella strains associated with human urinary tract infection. Infection and Immunity, 60(3), pp.1187-1192.

Tayel, A. et al., 2011. Antibacterial Action of Zinc Oxide Nanoparticles against Foodborne Pathogens. Journal of Food Safety, 31(2), pp.211-218.

Thangeeswari, T., George, A.T. & Arun Kumar, A., 2016. Optical properties and FTIR studies of cobalt doped ZnO nanoparticles by simple solution method. *Indian Journal of Science and Technology*, 9(1).

Thomas, S., Britto, S.J., Mathiew, S. and Mani, B., 2014. Evaluation of antibacterial potential of silver nanoparticles (SNPs) produced using rhizome extract of *Hedychium coronarium* J. Koenig. *International Journal of Pharmacy and Pharmaceutical Sciences*, 6(10), pp. 92-95.

Tiwari, V. et al., 2018. Mechanism of Anti-bacterial Activity of Zinc Oxide Nanoparticle Against Carbapenem-Resistant *Acinetobacter baumannii*. *Frontiers in Microbiology*, 9.

Tomás, J., Benedí, V., Ciurana, B. and Jofre, J., 1986. Role of capsule and O antigen in resistance of *Klebsiella pneumoniae* to serum bactericidal activity. *Infection and Immunity*, 54(1), pp.85-89.

Trautmann, M. et al., 1997. O-antigen seroepidemiology of Klebsiella clinical isolates and implications for immunoprophylaxis of Klebsiella infections. *Clinical Diagnostic Laboratory Immunology*, 4(5), pp.550-555.

Umar, H., Kavaz, D. and Rizaner, N., 2018. Biosynthesis of zinc oxide nanoparticles using *albizia lebbeck* stem bark, and evaluation of its antimicrobial, antioxidant, and cytotoxic activities on human breast cancer cell lines. *International Journal of Nanomedicine*, 14, pp.87–100.

van Duin, D. et al., 2015. Residence in Skilled Nursing Facilities Is Associated with Tigecycline Nonsusceptibility in Carbapenem-Resistant *Klebsiella pneumoniae*. *Infection Control & Hospital Epidemiology*, 36(8), pp.942-948.

Varadavenkatesan, T. et al., 2019. Photocatalytic degradation of Rhodamine B by zinc oxide nanoparticles synthesized using the leaf extract of *Cyanometra ramiflora*. *Journal of Photochemistry and Photobiology B: Biology*, *199*, pp.1-8.

Vielkind, M., Kampen, I. and Kwade, A., 2013. Zinc Oxide Nanoparticles in Bacterial Growth Medium: Optimized Dispersion and Growth Inhibition of *Pseudomonas putida*. *Advances in Nanoparticles*, 02(04), pp.287-293.

Wahab, R. et al., 2013. ZnO Nanoparticles Induces Cell Death in Malignant Human T98G Gliomas, KB and Non-Malignant HEK Cells. Journal of Biomedical Nanotechnology, 9(7), pp.1181-1189.

Wang, G., Zhao, G., Chao, X., Xie, L. and Wang, H., 2020. The Characteristic of Virulence, Biofilm and Antibiotic Resistance of Klebsiella pneumoniae. International Journal of Environmental Research and Public Health, 17(17), p.6278.

Wang, Y. et al., 2012. Differentiation in MALDI-TOF MS and FTIR spectra between two closely related species Acidovorax oryzae and Acidovorax citrulli. BMC Microbiology, 12, p. 182.

Webster, T. and Seil, I., 2012. Antimicrobial applications of nanotechnology: methods and literature. International Journal of Nanomedicine, 7(2012), p.2767.

Who.int. 2017. WHO publishes list of bacteria for which new antibiotics are urgently needed. [online] Available at: <https://www.who.int/news/item/27-02-2017-who-publishes-list-of-bacteria-for-which-new-antibiotics-are-urgently-needed> [Accessed 23 August 2021].

Wood, B. et al., 1998. FTIR microspectroscopic study of cell types and potential confounding variables in screening for cervical malignancies. Biospectroscopy, 4(2), pp.75-91.

Ye, Q. et al., 2020. Iron and zinc ions, potent weapons against multidrug-resistant bacteria. Applied Microbiology and Biotechnology, 104(12), pp.5213-5227.

Yoshida, K et al., 2001. Induction of interleukin-10 and down-regulation of cytokine production by Klebsiella pneumoniae capsule in mice with pulmonary infection. Journal of Medical Microbiology, 50(5), pp.456-461.

Yoshida, K. et al., 2000. Role of bacterial capsule in local and systemic inflammatory responses of mice during pulmonary infection with Klebsiella pneumoniae. Journal of Medical Microbiology, 49(11), pp.1003-1010.

Yusof, H. M., Mohamad, R. and Zaidan, U. H., 2020. Sustainable microbial cell nanofactory for zinc oxide nanoparticles production by zinc-tolerant probiotic Lactobacillus plantarum strain TA4. Microbial Cell Factories, 19(1), pp.1-17.

Zhang, L., Ding, Y., Povey, M. and York, D., 2008. ZnO nanofluids – A potential antibacterial agent. Progress in Natural Science, 18(8), pp.939-944.

Zhang, L., Jiang, Y., Ding, Y., Povey, M. and York, D., 2006. Investigation into the antibacterial behaviour of suspensions of ZnO nanoparticles (ZnO nanofluids). Journal of Nanoparticle Research, 9(3), pp.479-489.

APPENDICES

Appendix A

List of Equipment

Table A: Equipment and their brand/ model.

Equipment	Brand/ Model
Analytical balance	A&D HR-250AZ
Bunsen burner	Campingz, France
Cuvette	Greenier Bio -One
Falcon tube (15, 50 mL)	Nest Lab. Malaysia
Flat bottom 96 well microplate	Nest Biotechnology Co., Ltd., China
Fourier Transform Infrared Spectrophotometer (FTIR)	Perkin-Elmer Spectrum RX1, USA
Freeze dryer	Christ Alpha 1-4 LD
Lamina flow cabinet	ESCO SVC -4A1
Measuring cylinder	Bornex, China
Microcentrifuge tubes	Lifetech Synergy, Malaysia
Micropipette set and tips	Dragon Lab, USA
Microplate reader	FLUOstar® Omega, Germany
Petri dish	Nest Lab, Malaysia
Pipette Controller	Blue-Ray Biotech BlueSwan, Taiwan
Refrigerated centrifuge machine	SIGMA 1-14K, Germany
Scanning electron microscope with energy dispersive X-ray (SEM-EDX)	JOEL JSM 6710F, Japan
Schott bottle	DURAN, Germany
Spectrophotometer	Genesys 20, Thermo Scientific
10ml Disposable Syringe Without Needle, Luer Lock Tip	Terumo Philippines Corporation, Philippines
25mm syringe filter	Membrane Solutions, US

APPENDICES

Appendix B

List of Chemicals / Reagents

Table B: Chemicals/ reagents and their manufacturer/ brand.

Chemicals / Reagents	Manufacturer/ Brand
Absolute ethanol	Chem Solution Sdn. Bhd., Malaysia
Chloramphenicol	Bio Basic Canada Inc., USA
Erythromycin	Sigma-Aldrich, USA
Glutaldehyde, 25%	Acros Organics, USA
INT powder	HiMedia Laboratories Pvt. Ltd., India
Kanamycin sulfate	Bio Basic Canada Inc., USA
Tetracycline hydrochloride	Bio Basic Cnada Inc., USA
Tryptic Soy agar	Merck KGaA, Darmstadt, Germany
Tryptic Soy broth	Merck KGaA, Darmstadt, Germany
Zinc Oxide Nanoparticles (ZnO NPs)	Sigma- Aldrich, USA

APPENDICES

Appendix C

One-Way ANOVA for Turbidity Assay

Table C: Statistical analysis for percentage of inhibition obtained from the turbidity assay.

Sample (I)	Sample (J)	Mean Difference (I-J)	Significance
ZnO NP concentration (µg/mL)			
0.00	5.00	-4.89*	0.003
	10.00	-13.27*	0.014
	20.00	-18.78*	0.038
	40.00	-22.40*	0.027
	80.00	-25.60*	0.001
	160.00	-33.86*	0.015
	320.00	-47.84*	0.003
	640.00	-64.11*	0.002
	1280.00	-82.20*	0.002
	2560.00	-87.39*	0.002
	TCH (1 mg/mL)	-93.69*	0.000

*. The mean difference is significant at the 0.05 level.

APPENDICES

Appendix D

One-Way ANOVA for INT Assay

Table D: Statistical analysis for percentage of inhibition obtained from the INT assay.

Sample (I)	Sample (J)	Mean Difference (I-J)	Significance
ZnO NP concentration (µg/mL)			
0.00	5.00	-5.47*	0.005
	10.00	-12.06*	0.000
	20.00	-16.20*	0.000
	40.00	-22.97*	0.000
	80.00	-31.92*	0.000
	160.00	-38.49*	0.000
	320.00	-44.58*	0.000
	640.00	-65.82*	0.000
	1280.00	-83.55*	0.000
	2560.00	-87.29*	0.000
	TCH (1 mg/mL)	-93.97*	0.000

*. The mean difference is significant at the 0.05 level.

APPENDICES

Appendix E

Turnitin Report

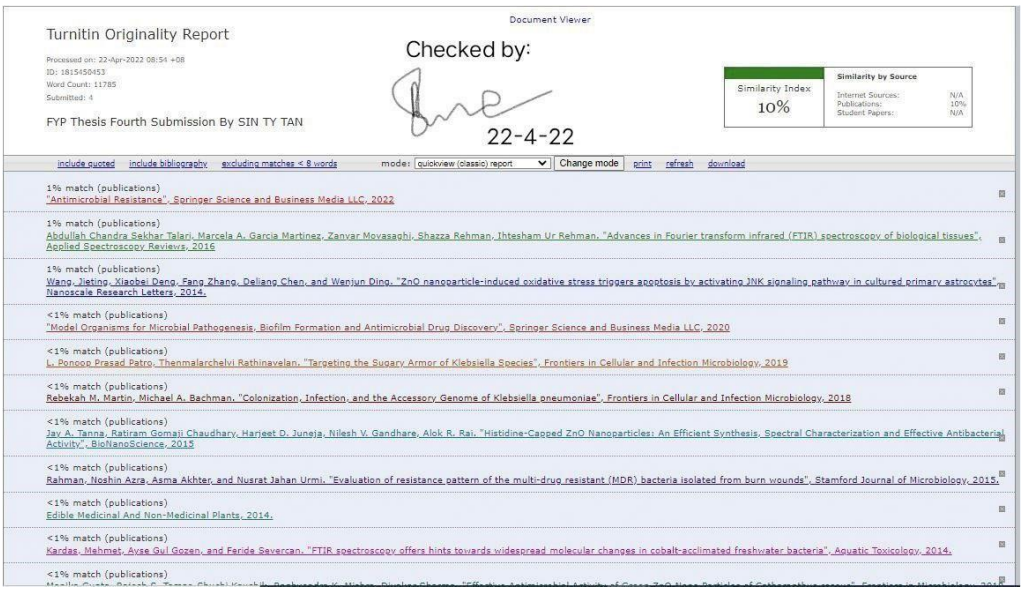

Document Viewer

Turnitin Originality Report

Processed on: 22-Apr-2022 08:54 +08
ID: 1815450453
Word Count: 11785
Submitted: 4

FYP Thesis Fourth Submission By SIN TY TAN

Checked by:

22-4-22

Similarity Index	Similarity by Source	
10%	Internet Sources:	N/A
	Publications:	10%
	Student Papers:	N/A

include quoted | include bibliography | excluding matches < 8 words | mode: quickview (classic) report | Change mode | print | refresh | download

1% match (publications)
"Antimicrobial Resistance", Springer Science and Business Media LLC, 2022

1% match (publications)
Abdullah Chandra Sekhar Talari, Marcela A. Garcia Martinez, Zanyar Movasaghi, Shazza Rehman, Ihtesham Ur Rehman, "Advances in Fourier transform infrared (FTIR) spectroscopy of biological tissues", Applied Spectroscopy Reviews, 2016

1% match (publications)
Wang, Jieting, Xiaobei Deng, Fang Zhang, Deliang Chen, and Wenjun Ding. "ZnO nanoparticle-induced oxidative stress triggers apoptosis by activating JNK signaling pathway in cultured primary astrocytes". Nanoscale Research Letters, 2014.

<1% match (publications)
"Model Organisms for Microbial Pathogenesis, Biofilm Formation and Antimicrobial Drug Discovery", Springer Science and Business Media LLC, 2020

<1% match (publications)
L. Ponpoo Prasad Patro, Thenmalarchelvi Rathinavelan, "Targeting the Sugary Armor of Klebsiella Species", Frontiers in Cellular and Infection Microbiology, 2019

<1% match (publications)
Rebekah M. Martin, Michael A. Bachman, "Colonization, Infection, and the Accessory Genome of Klebsiella pneumoniae", Frontiers in Cellular and Infection Microbiology, 2018

<1% match (publications)
Jay A. Tanna, Ratiram Gomaji Chaudhary, Harjeet D. Juneja, Nilesh V. Gandhare, Alok R. Rai, "Histidine-Capped ZnO Nanoparticles: An Efficient Synthesis, Spectral Characterization and Effective Antibacterial Activity", BioNanoScience, 2015

<1% match (publications)
Rahman, Noshin Azra, Asma Akhter, and Nusrat Jahan Urmi. "Evaluation of resistance pattern of the multi-drug resistant (MDR) bacteria isolated from burn wounds". Stamford Journal of Microbiology, 2015.

<1% match (publications)
Edible Medicinal And Non-Medicinal Plants, 2014.

<1% match (publications)
Kardas, Mahmet, Ayse Gul Gozen, and Farida Severcan. "FTIR spectroscopy offers hints towards widespread molecular changes in cobalt-acclimated freshwater bacteria". Aquatic Toxicology, 2014.

<1% match (publications)

APPENDICES

Appendix F

Turnitin Originality Report

Universiti Tunku Abdul Rahman			
Form Title: Supervisor 's Comments on Originality Report Generated by Turnitin for Submission of Final Year Project Report (for Undergraduate Programmes)			
Form Number: FM-IAD-005	Rev No.: 1	Effective Date: 3/10/2019	Page No.: 1of 1

FACULTY OF SCIENCE

Full Name(s) of Candidate(s)	TAN SIN TY
ID Number(s)	1904386
Programme / Course	BM
Title of Final Year Project	ANTIBACTERIAL PROPERTIES OF ZINC OXIDE NANOPARTICLES ON *Klebsiella pneumoniae* ATCC 13883

Similar ity	Supervisor 's Comments (Compulsory if parameters of originality exceeds the limits approved by UTAR)
Overall similarity index: 10 % Similar ity by source Internet Sources: N/A % Publications: 10 % Student Papers: N/A %	
Number of individual sources listed of more than 3% similarity: 0	

Parameters of originality required and limits approved by UTAR are as follows:
(i) Overall similarity index is 20% and below, and
(ii) Matching of individual sources listed must be less than 3% each, and
(iii) Matching texts in continuous block must not exceed 8 words
Note: Parameters (i) – (ii) shall exclude quotes, bibliography and text matches which are less than 8 words.

Note Supervisor/Candidate(s) is/are required to provide softcopy of full set of the originality report to Faculty/Institute

Based on the above results, I hereby declare that I am satisfied with the originality of the Final Year Project Report submitted by my student(s) as named above.

Signature of Supervisor
Name: Dr Sinouvassane Djearamane
Date: 22/04/2022

Signature of Co-Supervisor
Name:
Date: